Diverse muscle spindle firing properties emerge from multiscale muscle mechanics

[1,2]Kyle P. Blum, [3]Kenneth S. Campbell, [2]Brian C. Horslen, [4]Paul Nardelli, [4]Stephen N. Housley, [2,4]Timothy C. Cope, [2,5]Lena H. Ting

[1]Department of Physiology
Feinberg School of Medicine
Northwestern University
Chicago, IL 60611
USA

[2]Coulter Department of Biomedical Engineering
Emory University and Georgia Institute of Technology
Atlanta, GA 30322
USA

[3]Department of Physiology
University of Kentucky
Lexington, KY 40536
USA

[4]School of Biological Sciences
Georgia Institute of Technology
Atlanta, GA 30306
USA

[5]Department of Rehabilitation Medicine
Emory University
Atlanta, GA 30322
USA

ABSTRACT

Sensory information about the body's mechanical interactions with the environment are critical for neural control of movement. Muscle spindle sensory neurons richly innervate muscles in vertebrates; their firing patterns as muscles stretch have been well-characterized experimentally, but have not been fully explained mechanistically. Here, we show that a diverse range of muscle spindle firing characteristics are emergent from first principles of muscle contractile mechanics. We develop a mechanistic muscle spindle model that predicts well-known phenomena such as variations in muscle spindle sensitivity due to prior movement history and nonlinear scaling with muscle stretch velocity. The model further predicts how central commands to muscle spindles–fusimotor drive–alters their firing responses, and shows how seemingly paradoxical muscle spindle firing during voluntary force production in humans can arise. Our multiscale muscle spindle model provides a unifying biophysical framework that may broadly explain and predict movement-related sensory signals in health and disease.

INTRODUCTION

Precise movements depend on sensory information from throughout the body. Vertebrates have specialized sensors called muscle spindles that are widely distributed throughout skeletal muscles, providing critical information for all movements–from basic knee-jerk reflexes to playing musical instruments. Muscle spindles are all the more remarkable because they are not simply passive sensors: muscle spindles contain specialized muscle fibers that, when activated by central motor commands, alter the sensory information received by the nervous system. Despite decades of research, we still lack a mechanistic framework capable of explaining and predicting how movement-related biomechanical signals are transformed into the broad diversity of muscle spindle firing patterns observed experimentally, particularly in naturalistic behaviors. Developing a mechanistic framework for understanding how muscle spindle organs generate the complex sensory signals observed during movement will be critical for understanding not only the functional role of muscle spindles as proprioceptive sensors, but also neural control of movement and how it is affected by neurological disorders.

We recently demonstrated that a combination of muscle fiber force and yank, i.e. the first time derivative of force[1], matches the profile of muscle spindle firing throughout the stretch of a relaxed muscle[2,3]. The role of muscle mechanics and force in muscle spindle function has long been discussed[4,5], but not integrated into a mechanistic framework. We first used a phenomenological approach to demonstrate the parallel dependence of muscle spindle firing and muscle mechanics on prior movement of the muscle. Muscle spindle firing rates, together with muscle force and yank are high when the muscle is stretched after being held at a constant length, and lower if the muscle was moving prior to stretch[6]. In both cases, the length changes of the muscle-tendon unit are controlled to be the same, and muscle spindle firing rates vary in direct proportion to muscle fiber force and yank. These changes in muscle force and yank can be directly attributed to a type of history-dependence in resistive muscle force and yank, known as muscle[7].

We were inspired to test whether a muscle spindle model based on first principles of muscle biophysics could simulate muscle spindle firing during muscle stretch. Current muscle spindle models cannot simulate history dependence[8-11]. We reasoned that the mechanics of intrafusal muscle fibers within

the muscle spindle give rise to the history-dependent muscle spindle firing behaviors described above. History-dependent muscle forces have been simulated previously based on biophysical mechanisms of muscle force, such as the cycling crossbridge population kinetics[12,13]. We explicitly simulated the forces based on crossbridge mechanics of two intrafusal muscle fibers within the muscle spindle that are stretched in parallel. We assumed the driving potential of the muscle spindle to be proportional to the force and yank of each of the fibers to estimate receptor potentials[14,15], based on the idea that the nuclear region around which the muscle spindle ending is wrapped stretches linearly with intrafusal force[10,16]. We further hypothesized that different muscle spindle firing phenotypes in response to the same muscle stretch could be explained by varying the sensitivity of each muscle spindle's receptor potential to intrafusal fibers force and yank.

Once tuned to produce history-dependent responses to stretch[6], we tested whether our neuromechanical muscle spindle model could also predict other well-known properties of muscle spindle firing demonstrated experimentally. Using a single, nominal set of parameters, we tested whether a variety of classical muscle spindle firing characteristics would emerge, including: nonlinear relationship to stretch velocity[17], history-dependence[6], and increased firing due to gamma motor neuron activation[18,19]. In other muscle spindle model, nonlinear scaling of muscle spindle firing to stretch velocity has been empirically modeled[8]. Similarly, the effects of gamma motor neuron drive have been modeled phenomenologically based on experimental relationships between gamma motor activation and increased muscle spindle firing rates during stretch[8], or based on phenomenological models of muscle[9-11]. In contrast, we explicitly modeled the crossbridge mechanism causing increased muscle spindle sensitivity to stretch under gamma motor activation[13].

Finally, we tested whether seeming paradoxical muscle spindle firing observed in humans during voluntary force production when muscles fibers are isometric or shortening would also emerge from a biophysical model[20,21]. In the relaxed muscle, muscle spindles lengthen and fire when they are stretched. In active movement, central drive via gamma motor neurons can stretch the muscle spindle encoding region independent of the stretch of the parent muscle. Arguably, the role of central drive is one of the most

important, and yet poorly understood aspects of muscle spindle function in behavioral conditions[22]. Central drive is critical in understanding complex muscle spindle firing patterns observed during behavior and may underlie the variability and seemingly paradoxical muscle spindle firing when muscles are isometric[20] or shortening slowly in behaving conditions.

Overall, we demonstrate that a wide range of muscle spindle firing characteristics are emergent from the biophysical properties of intrafusal muscle fibers and their mechanical arrangement in the muscle. As such, our multiscale muscle spindle model provides a unifying biophysical framework based on first principles that can broadly explain muscle spindle firing activity in naturalistic conditions and the impact of neuromuscular disorders on sensory signals mediating movement.

RESULTS

Muscle fiber force and yank reproduce diverse passive features of rat muscle spindle IFRs.

We first demonstrated that muscle spindle firing rates in relaxed rat muscles can be quantitatively related to muscle fiber force and yank. We recorded muscle spindle IFRs in anesthetized rats while stretching the triceps surae muscles (Fig. 1). In the relaxed condition, we assumed that muscle fiber forces provide a reasonable proxy for resistive forces within the intrafusal muscle fibers that stretch the muscle spindle mechanosensory apparatus (Fig. 1). We previously demonstrated that whole musculotendon force in our rat experiments is not predictive of muscle spindle IFRs [3]. Only a portion of the total musculotendon force can be attributed to muscle fiber force, with the remaining nonlinear elastic component attributed to extracellular tissues[3,23]. The initial rise in muscle fiber force at the onset of stretch (Fig. 1, blue trace) – which is attributed to muscle crossbridge interactions – became more apparent once the extracellular tissue forces were subtracted from whole musculotendon force.

Like in cats[2], fine temporal details of rat muscle spindle firing could be reconstructed by pseudo-linear combinations of estimated intrafusal muscle fiber force and yank, including initial bursts, dynamic responses during ramps, rate adaptation during holds, and movement history-dependent firing (Fig. 2A-C; Fig. S1). The reconstructions revealed history-dependent initial bursts that were present in the first of consecutive stretch-shorten cycles correspond with a large, history-dependent yank component at the onset of stretch that is greatly reduced in subsequent stretches (Fig. 2B). The dynamic response during ramp stretches was primarily reconstructed by the force component (Fig. 2C), and was larger during the first stretch of a repeated sequence (Fig. 2B). Rate adaptation during the hold period was reconstructed by the force component in both slow and fast stretches (Fig. 2C)[17].

Muscle fiber force- and yank-based reconstruction of muscle spindle Ia firing rates was robust to experimental perturbations to the mechanosensory apparatus due to either oxaliplatin chemotherapy (OX) or electrical stimulation of the afferent (STIM). Muscle spindles in healthy rats treated with OX maintain an initial burst and dynamic response, but lack sustained firing during the hold period (Fig. 2D vs 2E; Fig.

100 S2)[24]. These phenotypes were primarily reconstructed by the yank component (Fig. 2D, blue trace), with a
101 small contribution of the force component (Fig 2D, red trace; Fig. S2). Conversely, electrical stimulation
102 (STIM) of the muscle spindle afferent in a healthy rat (500 ms duration, 100 Hz train of 30nA pulses)
103 reduced the initial burst and dynamic response during a stretch applied immediately after stimulation (Fig.
104 2F; Fig. S2). These phenotypes were primarily reproduced by the force component, with reduced
105 contributions of the yank component (Fig. S3). In each case we assumed that the muscle fiber force and
106 yank are not altered by the perturbation; rather, the neuronal sensitivity to either force or yank is
107 differentially affected by OX and STIM. These results demonstrate that force and yank sensitivity are not
108 necessarily coupled in the mechanotransductive process.

109 *Modifying neuronal sensitivity to force and yank generates and array of muscle spindle firing phenotypes.*
110 The apparently differential effects of oxaliplatin and axonal stimulation on spindle firing rates led us to
111 hypothesize there is a degree of independence in the transduction of force and yank in the spindle. We
112 further tested this hypothesis by simulating neuronal spiking arising from force- and yank-based driving
113 potentials (Fig 3A; see Methods). Nominal sensitivities of the model receptor currents (closely related to
114 driving potential) were chosen to reproduce a typical recorded muscle spindle firing rate during stretch (Fig
115 3B, green shaded box). We then generated a family of muscle spindle firing phenotypes (Fig. 3B, blue dots)
116 by systematically varying sensitivity of receptor currents (Fig. 3, thin black lines) to the same muscle fiber
117 force (Fig. 3B, vertical axis) and yank (Fig. 3B, horizontal axis) of the same stretch (Fig 3B).

118 Varying force- and yank- sensitivity generated diverse muscle spindle firing phenotypes observed
119 experimentally – including the OX and STIM phenotypes. Firing profiles exhibited larger initial bursts and
120 dynamic responses as yank sensitivity increased (Fig. 3B, left to right), consistent with classically-identified
121 dynamic muscle spindle phenotypes[25]. High force sensitivity led to profiles with elevated plateau firing
122 (Fig. 3B, top to bottom), consistent with classically-identified static muscle spindle phenotypes[25,26]. The
123 firing profiles with high yank and lowest force sensitivity resembled the OX firing phenotype[24] (Fig. 3B,
124 yellow shaded boxes, cf. Fig 2D) and the firing profiles with lowest yank sensitivity resembled the STIM

125 firing phenotype (Fig. 3B, red shaded boxes, cf. Fig 2D). We concluded that independently varying
126 neuronal sensitivity to force and yank explains a spectrum of spindle firing phenotypes.

127 *A muscle crossbridge model predicts intrafusal muscle fiber force and yank underlying muscle spindle*
128 *firing rates.*

129 We then built a biophysical model of muscle spindle mechanics to first predict intrafusal fiber force and
130 yank during muscle stretch conditions when experimental data are not readily available. Our mechanistic
131 muscle spindle model consists of a pair of half-sarcomere muscle models arranged in parallel, simulated
132 using two-state population actin-myosin interactions[13]. The simulated "dynamic" fiber loosely represented
133 the putative dynamic bag1 intrafusal muscle fibers, thought to mediate initial burst[27,28]. The simulated
134 "static" fiber loosely represented the bag2 and chain intrafusal muscle fibers of the muscle spindle thought
135 to mediate tonic firing (Fig. 4A)[29]. The dynamic fiber model was designed so that its force response during
136 eccentric contraction was greater than that of the static fiber, with a more compliant passive element than
137 the static fiber[30] (see Methods; Fig. S5). Length changes to the spindle were applied to both fibers equally.
138 Weighted, summed contributions of dynamic fiber force and yank and static fiber force were used to
139 simulate muscle spindle driving potential (Fig. 4A, lower panel; See Materials and Methods for more
140 details).

141 Our mechanistic model predicted a spectrum of muscle spindle firing phenotypes by varying the
142 sensitivity (gain) of driving potentials to biophysically-predicted intrafusal fiber force and yank (Fig. 4B).
143 The predicted muscle spindle firing phenotypes closely resembled biological firing phenotypes discussed
144 earlier. History-dependence in simulated dynamic and static fiber force and yank emerged from crossbridge
145 population dynamics (Fig 4C). If the fibers were preconditioned with a stretch, actin-myosin attachment
146 was reduced, leading to lower force and yank during stretch. Muscle shortening in our model can also cause
147 slack in the intrafusal muscle fibers, where the internal force and yank are zero.

148

149 *A biophysical muscle spindle model predicts a variety of classic muscle spindle firing phenomena.*

150 We then tested whether spindle firing characteristics under a broad range of muscle stretch conditions
151 previously reported in the literature were emergent from our biophysical model. We selected a few
152 examples to test whether observed muscle spindle firing characteristics were caused by muscle crossbridge
153 interactions underlying intrafusal muscle fiber force and yank. To eliminate neural dynamics as a source of
154 variability, we examined simulated driving potentials rather than firing rates.

155 In our model, the scaling properties of muscle spindle dynamic responses and initial bursts with
156 increasing stretch velocity are predicted to arise due to intrafusal crossbridge kinetics. In a series of constant
157 velocity stretches relative to optimal muscle length, L_0 (0.1 - 1.0 L_0/s in 0.1 L_0/s increments; Fig 5A), we
158 computed the "dynamic index", classically defined as the difference in firing rate between the end of the
159 ramp and after 0.5 s of isometric hold, which increases with stretch velocity (Fig. 5B-C[17]). We predicted a
160 sublinear increase in dynamic index with stretch velocity, emergent from intrafusal mechanics, resembling
161 the classically-reported fractional-power velocity relationship in muscle spindle firing rates (Fig. 5C[31]). In
162 the same simulations, linear scaling of initial burst amplitude with stretch acceleration was predicted[32,33].
163 Initial burst scaling was emergent from intrafusal muscle fiber yank at the onset of stretch due to the
164 elasticity of attached cross-bridges that then detach rapidly after being stretched a small fraction of L_0[34,35].
165 To our knowledge, neither of these phenomena has been previously demonstrated to arise from the same
166 mechanistic model.

167 Our biophysical model predicted history-dependent changes in the initial burst previously seen in
168 human, cat, rat, and toad experiments. In three consecutive, identical stretches, our model predicted an
169 initial burst and elevated dynamic response on the first, but not second stretch (Fig. 6A). In the third stretch,
170 the amplitude of the simulated driving potentials recovered asymptotically as the time interval between
171 stretches increased to 10s (Fig. 6A), resembling the recovery of spike counts during the dynamic response
172 in rates (Fig 6B) [6] and the recovery of initial bursts as a function of hold period in toads (Fig. 6B)[36]. Our
173 model predicted an initial burst at the onset of sinusoidal muscle stretches (Fig. 6C), consistent with
174 microneurographic recordings from awake humans (Fig. 6C).

175

176 *A biophysical muscle spindle model predicts effects of central drive on muscle spindle firing.*

177 The effects of gamma motor neuron activation on muscle spindle responses to stretch in relaxed muscle
178 also emerged from the mechanics of our intrafusal model. We simulated classic experiments in which
179 dynamic and static gamma motor neurons projecting to the muscle spindle were electrically stimulated in
180 anesthetized animals by increasing the number of available actin binding sites in simulated intrafusal static
181 and dynamic fibers, respectively (Fig. 7A). Consistent with prior findings, simulated dynamic gamma drive
182 increased the dynamic fiber force and yank during stretch, predicting increased driving potentials
183 underlying initial burst and dynamic responses and proportionally reduced baseline activity[19,37]. Increased
184 static fiber activation increased the baseline spindle activity, with smaller effects on the initial burst and
185 dynamic response (Fig. 7A-B)[18,19,38]. Even the paradoxical increase and decrease in dynamic index with
186 respective dynamic and static fusimotor stimulation reported previously (Fig. 7C left plot)[18,38] were
187 predicted by our model (Fig. 7C right plot).

188 Having simulated the effects of gamma drive on muscle spindle activity in a relaxed muscle, we
189 tested the ability of our mechanistic model to predict muscle spindle firing during isometric active
190 contractions (Fig 8)[21,39]. We simulated muscle spindle driving potentials (Fig. 8A) during constant or slowly
191 shortening muscle lengths (Fig. 8B) and constant or slowly increasing fusimotor activation (Fig. 8C) to
192 span the range of difficult-to-control experimental parameters such as fascicle shortening under isometric
193 conditions. Paradoxical increases to spindle firing rates were present during muscle shortening (Fig. 8A
194 green traces) when the negative effects on intrafusal force and yank caused by muscle shortening (Fig. 8B
195 green traces) were outweighed by the positive effects from fusimotor drive (Fig. 8C black trace). When
196 muscle shortening velocity was increased under these conditions (Fig. 8B orange traces), the interactions
197 of muscle shortening and fusimotor drive had a more complicated effect on muscle spindle firing (Fig. 8A
198 orange traces), which increased, decreased, or stayed the same depending on the rate of muscle shortening.
199 When fusimotor drive was not present (Fig. 8A-C dashed purple traces), muscle shortening always caused
200 a decrease in the predicted spindle firing rate. Our mechanistic model of spindle firing demonstrates the

complicated interaction between central drive and external loads on spindle output (Fig. 8D) and predicts the paradoxical of spindle firing behaviors demonstrated previously (Fig. 8E).

DISCUSSION

Our multiscale muscle spindle model provides a unifying biophysical framework that broadly explains and predicts movement-related sensory signals in health and disease. We demonstrate that the diverse range of muscle spindle firing characteristics – well-documented in the literature but not completely understood mechanistically – is emergent from first principles of intrafusal muscle contractile mechanisms. By explicitly simulating the biophysical force-generation mechanisms in intrafusal muscle fibers within the muscle spindle and converting the resultant force and yank to afferent driving potentials using a simple relationship, we predicted muscle spindle firing in a broad range of behaviorally-relevant conditions. The complex interactions of external loads, muscle activation, and fusimotor drive all contribute to the firing rates of muscle spindle afferents and can create firing patterns that may be considered paradoxical when considering muscle spindles as simple passive sensors. However, these variables are consistently reflected in the force and yank of intrafusal muscle fibers which determine the stretch of the elastic equatorial encoding region in the muscle spindle. We arrive at a simple unifying hypothesis of muscle spindle function in sensorimotor control as muscle-centric exafference sensors reflecting the interplay of external and self-generated motion and force occurring during naturalistic movements. As such, our biophysical muscle spindle model provides a mechanistic, predictive, and extendable framework for understanding how properties of tissues, muscles, neurons, and central drive affect muscle spindle sensory function in both health and impairment.

Generalizability of biophysical modeling approach

Our approach of starting with biophysical principles enabled us to develop a muscle spindle model that predicts muscle spindle firing properties beyond the conditions that it was designed to replicate, without any change in model parameters. Specifically, we incorporated the biophysical properties of muscle

227 crossbridge kinetics, to produce the muscle fiber force and yank that drive history-dependent responses to
228 a repeated stretch stimulus, including the initial burst. Other muscle spindle models do not exhibit history-
229 dependence and – by design – either lack[11] or always generate[8] an initial burst at the onset of stretch. In our
230 model, the initial burst emerges from the large number of crossbridges that are attached after a period of
231 rest, temporarily increasing the stiffness of the fibers before being stretched to their mechanical limit. This
232 number depends on the prior and current fiber length, velocity, acceleration, and activation of the intrafusal
233 fibers, and thus leads to the modulation of the initial burst of the spindle afferent with these variables.
234 Similarly, the fractional power relationship between muscle spindle dynamic responses and stretch
235 velocity[8,9] has typically been imposed by including it explicitly within the model definition. While it can
236 be simulated using a phenomenological muscle model with a built-in fractional power function, these
237 models fail to account for the history dependence of the velocity sensitivity and thus fail to replicate muscle
238 spindle firing patterns outside of tightly controlled laboratory conditions. Here, history dependence, the
239 nonlinear relationship to stretch velocity, and the scaling of the initial burst to acceleration are all implicit,
240 emergent properties of intrafusal crossbridge force and yank under different conditions – no explicit
241 formulation of these relationships is necessary. Finally, most prior models have static parameter sets meant
242 to mimic discrete experimental conditions, such as constant gamma drive, limiting their generalizability to
243 behavioral conditions where both static and dynamic gamma drive may vary as a function of time. By taking
244 a structural approach to the interactions between intrafusal and extrafusal muscle fibers the effect of gamma
245 motor drive can be more robustly simulated[9].

246 Building from the core framework presented here, a biophysical muscle spindle model may enable
247 predictions of muscle spindle signals during naturalistic movement conditions in health and disease. We
248 provide only the initial modeling framework for the muscle spindle, which could be further developed to
249 have more detailed and muscle-specific parameters[13]. Ultimately, integration into musculoskeletal
250 simulations would enable hypotheses about gamma motor drive in normal and impaired movement to be
251 tested[40,41]. Importantly, our model could be extended to include the effects of multiscale mechanisms on
252 muscle spindle firing, from architectural arrangement of the muscle spindle within the muscle [42], intra- and

253 extrafusal muscle myosin expression, extracellular matrix stiffness, mechanosensory encoding
254 mechanisms, and biophysical neural dynamics. As such, the encoding of muscle fiber force and yank
255 provides a unifying, mechanistic framework for approaching a broad range of previously unanswered
256 questions about proprioceptive function in health and disease.
257
258 *Sensitivity to intrafusal force and yank parsimoniously explains the diversity of muscle spindle firing*
259 *phenotypes in both passive and active movement conditions*
260 The principle of muscle spindle sensitivity to intrafusal force and yank parsimoniously explains
261 variations in firing profiles across different muscle spindle Ia afferents demonstrated experimentally in
262 different active and passive conditions. A continuum of muscle spindle firing phenotypes has been observed
263 in relaxed muscle, absent central drive from motor neurons, within and across muscles, species, and in
264 health and disease. Differences in static firing rate, dynamic firing rate, initial burst, and several other
265 summary variables identified under specific stretch conditions have been used to classify muscle spindles,
266 but these measures are superficial, difficult to compare, and of limited use in predicting muscle spindle
267 firing in naturalistic behaviors. Our results suggest that intrafusal muscle fiber force and yank profiles
268 robustly drive the dynamics of muscle spindle driving potentials across a variety of conditions. The few
269 available recordings of muscle spindle receptor potentials during muscle stretch exhibit fast initial transients
270 similar to muscle fiber yank, as well as a sustained potential that resembles muscle force and its relaxation
271 when stretched. We show that sweeping a range of neural sensitivities to intrafusal force and yank predicts
272 a range of firing phenotypes resembling those seen previously in both healthy and perturbed conditions.
273 Further, each set of sensitivities can predict muscle spindle firing across different stretch velocities and
274 displacements. Our results provide the first mechanistic and quantitative evidence for the long-discussed
275 idea that muscle spindle firing rates are driven by the dynamics of muscle fiber forces[16]. Whether a similar
276 principle describes the firing of the second type of muscle spindle afferent, group II's, remains to be tested.
277 Sensitivity to intrafusal fiber force and yank further explains how muscle spindles alter their firing
278 profiles by central drive during both muscle stretch and active muscle contraction. Central drive to muscle

279 spindles via gamma motoneurons causes intrafusal muscle fibers to contract in their polar regions,
280 increasing intrafusal muscle fiber force that stretches the equatorial region[43]. At the same time, the length
281 of the entire muscle spindle is determined by the force balance between the environmental loads and the
282 total extrafusal muscle force. As a result of these interactions, our biophysical model can reflect aspects of
283 whole muscle force and yank, length, stiffness, velocity, or acceleration, consistent with findings in the rich
284 muscle spindle literature. For example, tonic gamma drive to the simulated "static fiber" increases tonic
285 background activity of the muscle spindle in proportion to force while the total muscle length remained
286 unchanged; this increase in background firing rate has been interpreted as an increase in sensitivity to whole
287 muscle-tendon length[22]. In contrast, tonic gamma drive to the simulated "dynamic fiber" primarily
288 increased the resistive force and yank of the intrafusal fiber during stretch, due to transient changes muscle
289 fiber stiffness. This resulted in increased muscle spindle dynamic responses during ramp stretches, which
290 has been explained as increased sensitivity to whole muscle-tendon velocity[22]. Here we further demonstrate
291 the apparent sensitivity of the initial burst to acceleration[2] also increases with dynamic gamma drive due to
292 increase in muscle stiffness prior to movement. Finally, the adaptation of muscle spindle firing rates when
293 held at a constant length after stretch follows the decrease in force of the intrafusal muscle fiber when it is
294 held at a constant length[2,44]. During active muscle contraction, a common central signal to the parent muscle
295 and the muscle spindle, such as in the case of alpha-gamma coactivation, could cause muscle spindle firing
296 to increase, decrease, or remain unchanged depending on the relative amount and rate of shortening in the
297 parent muscle in reference to changes in intrafusal fiber force due to gamma drive and intrinsic mechanics
298 (Fig 8).
299
300 *Muscle spindles signal interactions between external forces and central drive*
301 Amidst the complex interplay between central drive and environmental forces there is a surprisingly
302 simple unifying hypothesis of muscle spindle function in sensorimotor control: they serve as muscle-centric
303 exafference sensors. In a simple agonist-antagonist system, the concentric, or shortening, contraction of the
304 agonist will stretch the passive muscle spindles within the opposing antagonist muscle; firing in the

antagonist muscle spindle signals the passive force or movement caused by contraction of the agonist muscle. If, in a similar scenario, a load prevents the agonist from shortening, there would be no change in the muscle spindle afferent activity in the antagonist, signifying a lack of movement. However, the muscle spindle afferent in the agonist muscle would increase its firing due to fusimotor drive. In both cases, the muscle, whether an agonist or antagonist, fires when interacting with a muscle-exafferent force, i.e. one that originates outside the parent muscle. Muscle spindles as muscle-centric exafference sensors is an idea consistent with other non-traditional views of muscle spindle function, including its role in perception of weight[45,46] where mismatches in extrafusal and intrafusal mechanical state due to fatigue or pre-conditioning alter the perception of both force and position[47,48].

Understanding the complex nature of muscle afferent signals as they relate to internal and external forces is necessary for determining their functional roles in dynamic tasks. For example, in locomotion, muscle spindles can appear to follow both external and self-generated motion and force. During the swing phase of gait in the cat, ankle extensor muscles are relaxed and stretched by gravitational forces; Ia firing rates follow muscle velocity and/or length[49,50], which closely resemble muscle force and yank[2] in passive conditions. However, the same muscle spindle also fires in early stance when the muscle is active during limb loading but not changing length: this firing is likely due to intrafusal force generated by fusimotor drive (Fig. 8, green traces). Then, the muscle spindle ceases to fire in midstance, when the muscle is still activate, but is unloaded and shortening[49], tending to make the muscle spindle fall slack (Fig. 8, purple traces). Our multiscale model provides a mechanistic framework that can explain the rich diversity of movement-related biomechanical signals in naturalistic behaviors, enabling a more sophisticated understanding of muscle spindles as proprioceptive sensors, their role in neural control of movement, and how neurological disorders disrupt sensorimotor systems.

FIGURES

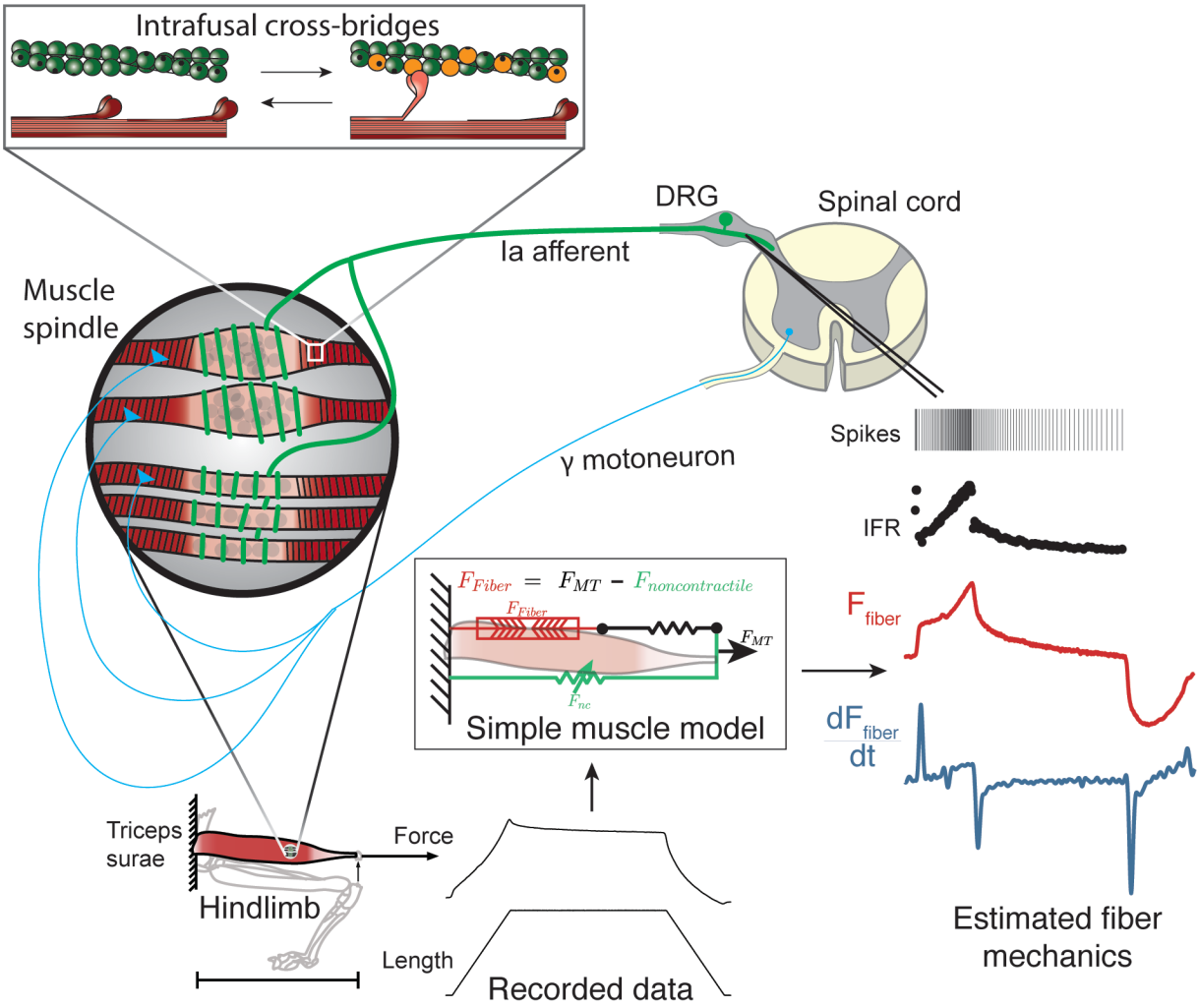

Figure 1 Overview of methodologies to test hypothesis that muscle spindle Ia afferent firing rates follow intrafusal muscle fiber force due to cross-bridge interactions. Ia afferent firing rates were recorded from dorsal rootlets during stretches of the triceps surae muscle in anesthetized rats. Muscle fiber forces were estimated by subtracting noncontractile forces from measured whole musculotendon force. The exponential rise in force with stretch was assumed to arise from non-contractile tissue in parallel with the muscle-tendon unit with exponential stiffness (Blum et al. 2019). The remaining estimated muscle fiber force and yank exhibited similar temporal characteristics to the muscle spindle IFR. Intrafusal muscle fiber force and yank were then simulated using a cross-bridge based model to predict muscle spindle IFRs.

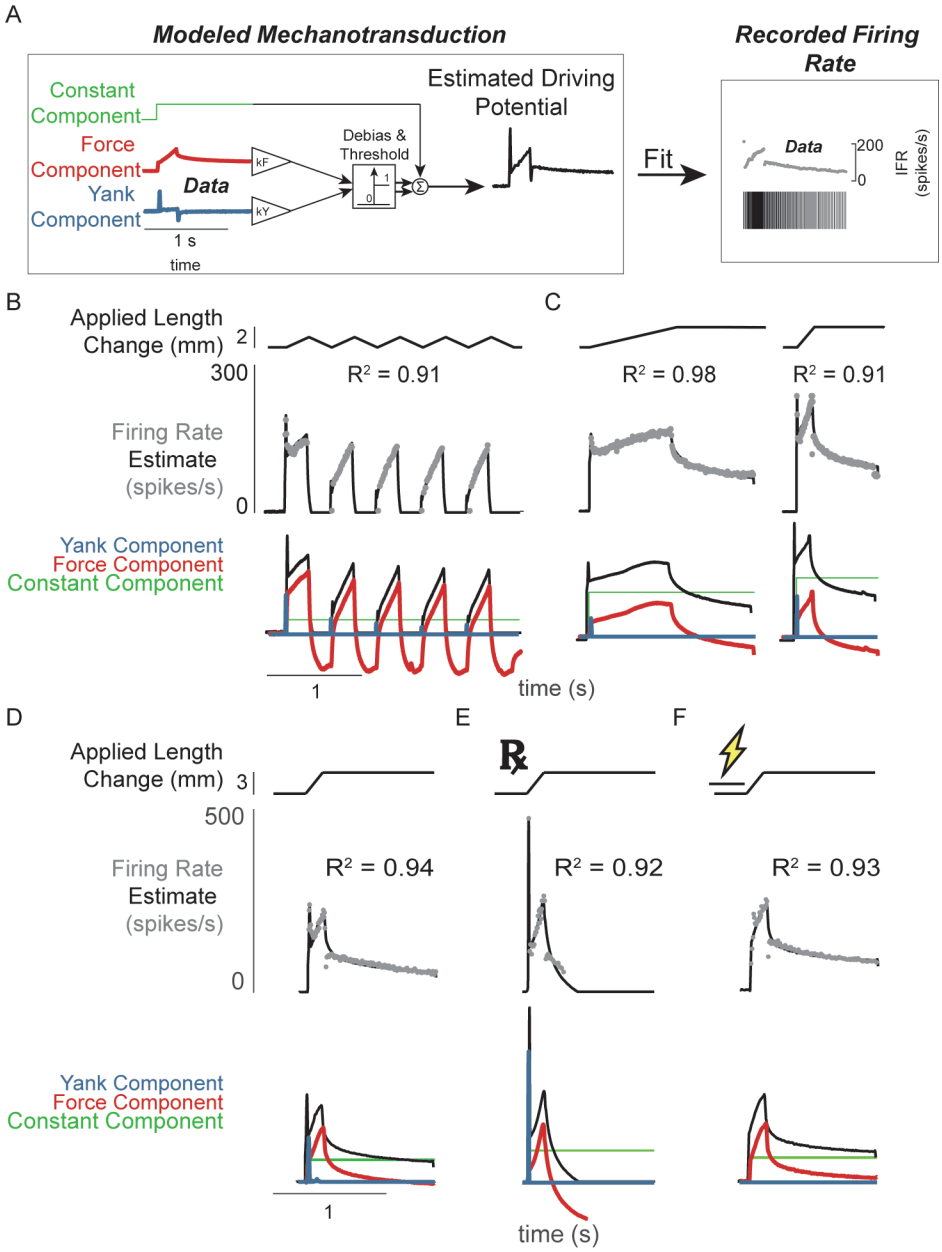

Figure 2 Muscle spindle driving potentials estimated from independent contributions of experimentally-derived muscle fiber force and yank. A) Estimated driving potentials were derived from linear combinations of muscle fiber force and yank, half-wave rectified, and compared against recorded muscle spindle Ia afferent firing rates. Weights of each component were optimized to match recorded spiking dynamics. B) Recorded muscle spindle Ia afferent firing rates (gray dots) in history-dependent conditions, having non-unique relationships to muscle length and velocity, were reproduced using muscle fiber force and yank (black lines). Notably, the initial burst and increased firing during ramp in the first stretch were attributed to increased muscle fiber yank and to greater force during the first stretch, respectively. C) Likewise, muscle fiber force and yank could also account for the temporal dynamics of Ia afferent firing in response to both slow and fast stretches. D) This model permits independent manipulation of the force and yank contributions to muscle spindle firing rates. As such, we can explain the altered muscle spindle Ia afferent firing patterns in E) oxaliplatin chemotherapy-

induced sensory neuropathy as a loss of force sensitivity, and F) after antidromic electrical stimulation of the axon as loss of yank sensitivity.

A

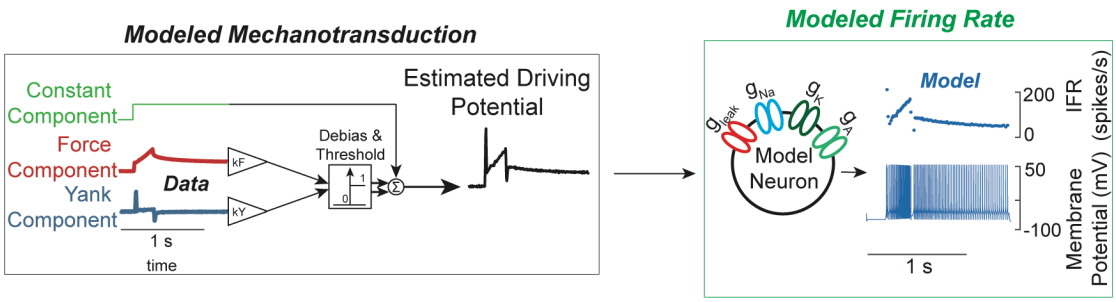

B

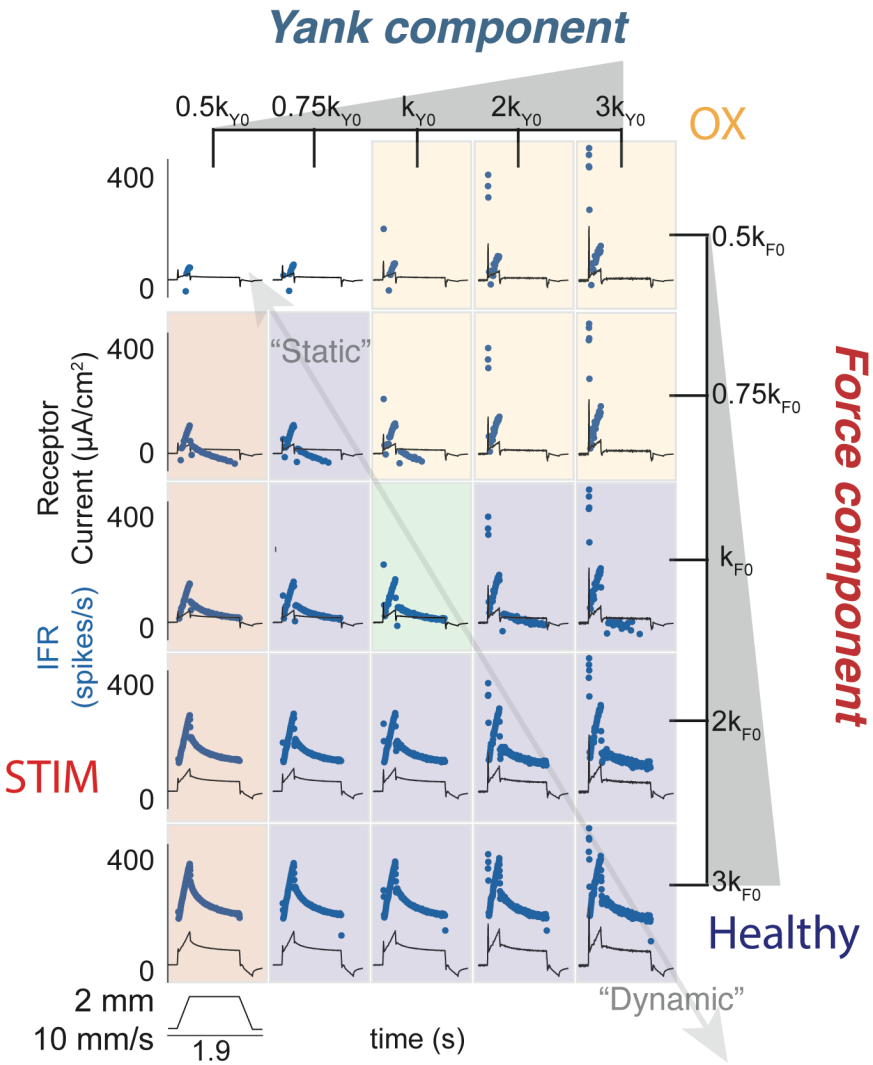

Figure 3 Spectrum of passive muscle spindle firing phenotypes accounted for by varying sensitivity to experimentally-derived muscle fiber force and yank. A) Sensitivity to experimentally-derived force and yank was systematically varied for a single stretch and resultant driving potentials were input to a Connor-Stevens model neuron to generate firing patterns. B) Nominal force and yank weights were identified to recreate experimentally-recorded muscle spindle response to a representative stretch (green box). Increasing sensitivity to yank (left to right) generated larger initial bursts and dynamic responses during the ramp, and resembled responses from oxaliplatin-treated specimens at the highest yank and lowest force

sensitivities (orange boxes, compare to Figure 2E). Increasing sensitivity to force (top to bottom) generated higher firing rates during the hold period and resembled Ia afferent firing responses after axonal stimulation at the lowest yank and highest force sensitivities (red boxes, compare to Figure 2F). Varying the weights of the force and yank sensitivities could recreate the spectrum of healthy muscle spindle firing profiles reported classically (purple boxes).

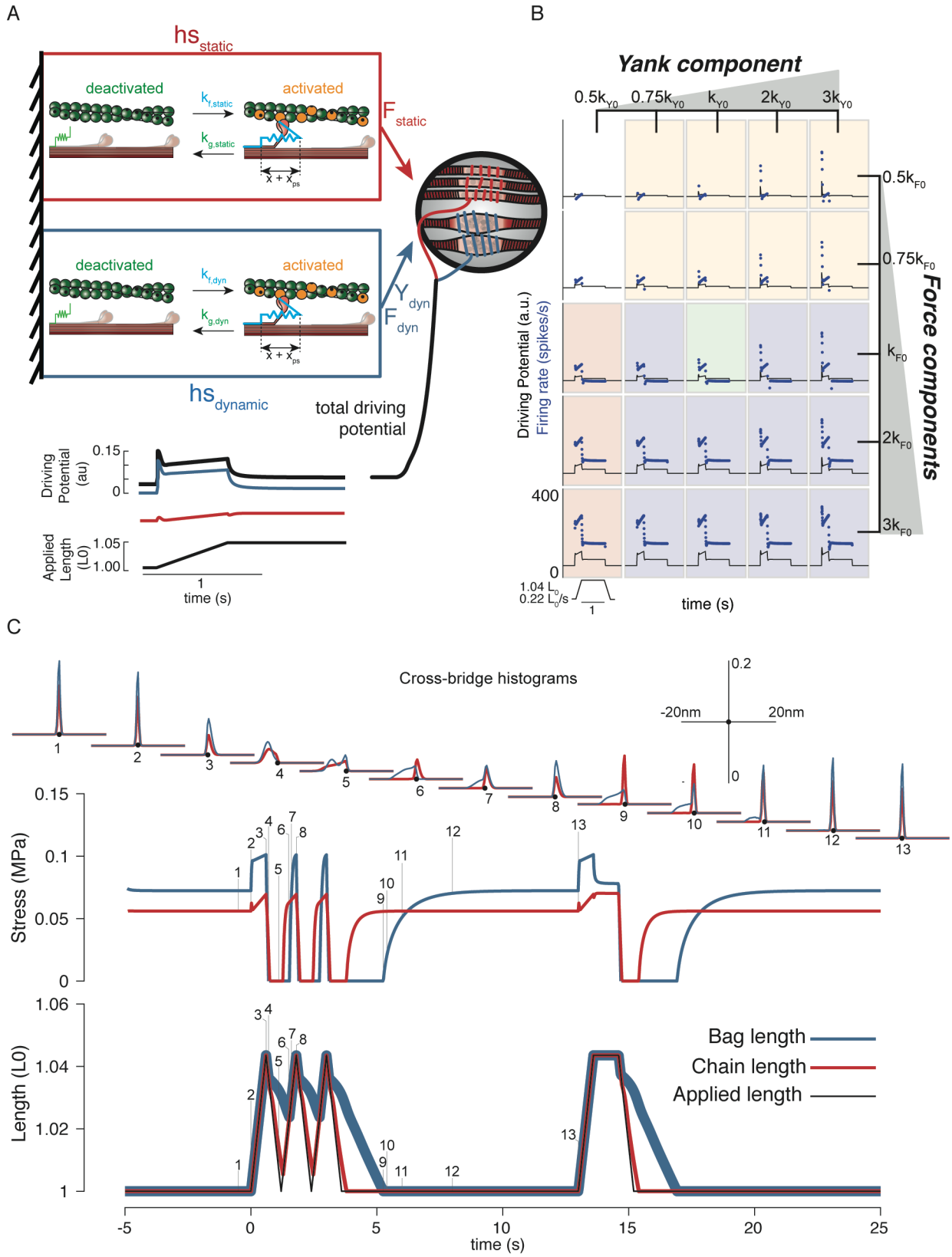
A
hs static
deactivated
activated
k f,static
k g,static
F static
x + x ps
deactivated
activated
k f,dyn
k g,dyn
Y dyn
F dyn
hs dynamic
total driving potential
Driving Potential (au)
0.15
0
Applied Length (L0)
1.05
1.00
1
time (s)
B
Yank component
0.5k Y0
0.75k Y0
k Y0
2k Y0
3k Y0
0.5k F0
0.75k F0
k F0
2k F0
3k F0
Force components
Driving Potential (a.u.)
Firing rate (spikes/s)
400
0
1.04 L0
0.22 L0/s
1
time (s)
C
Cross-bridge histograms
0.2
-20nm
20nm
0
Stress (MPa)
0.15
0.1
0.05
0
Length (L0)
1.06
1.04
1.02
1
Bag length
Chain length
Applied length
-5
0
5
10
15
20
25
time (s)

Figure 4 Generative model of muscle spindle driving potentials based on simulated muscle cross-bridge kinetics. A) The muscle spindle model consists of two muscle fibers in a parallel mechanical arrangement, loosely representing intrafusal bag and chain fibers. B) During stretch, force and yank of the "dynamic" fiber is linearly combined with force of the "static" fiber, with different proportions generating driving potentials consistent with "dynamic" and "static" muscle spindle firing response phenotypes. C) A population of myosin cross-bridges and their relative displacement and velocity with respect to active actin binding sites was simulated during three consecutive ramp-stretch-release stretches. The distribution of crossbridge lengths relative to actin binding sites is shown at different timepoints of imposed kinematics (numbered graphs and timepoints). The length of the dynamic and static fibers (lower trace) and the stress in the dynamic and static fibers (middle trace) is shown. Deviations between applied length and muscle fiber length occur due to muscle fiber slack.

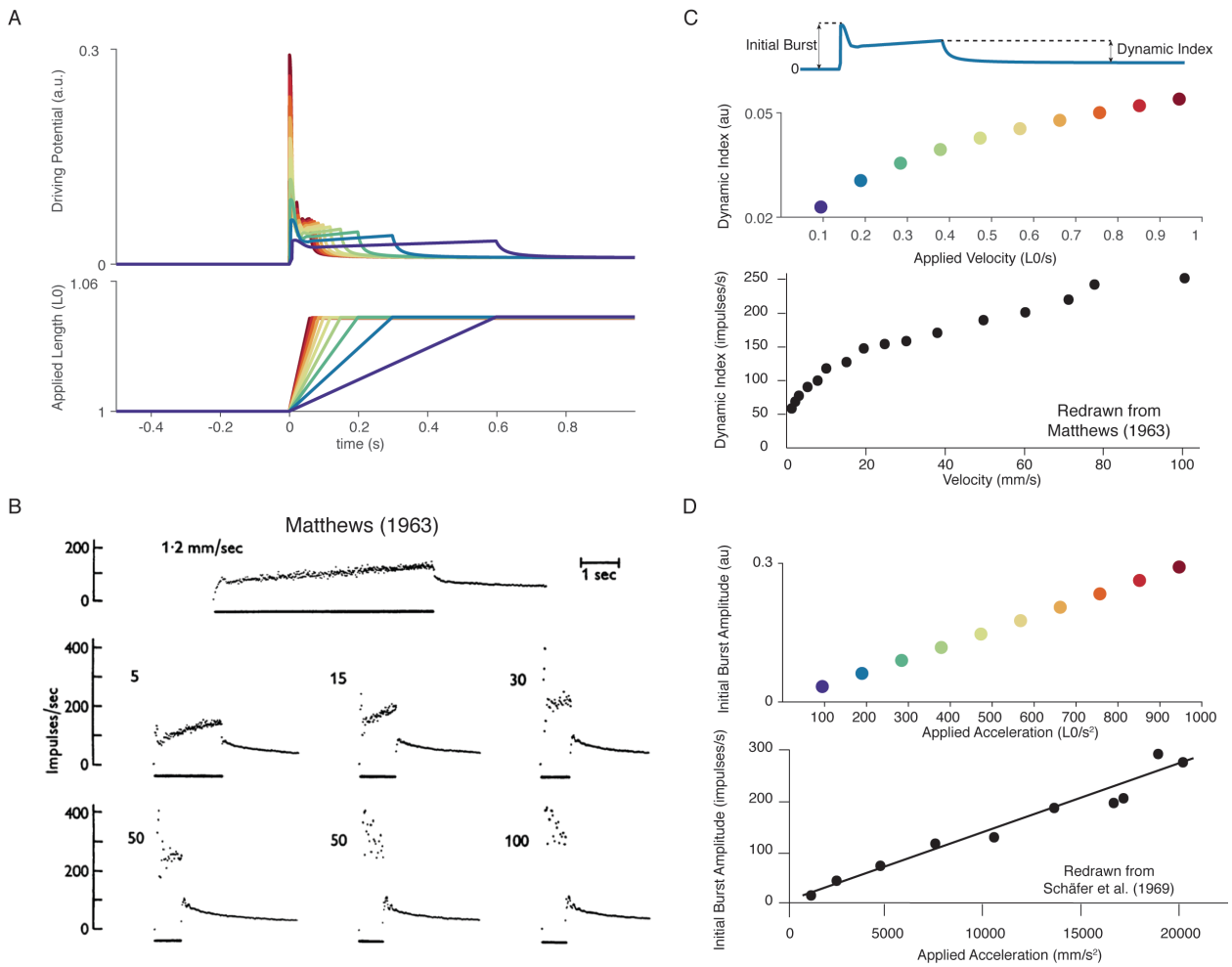

Figure 5 Muscle spindle firing dynamics emerge from crossbridge mechanisms during simulated muscle stretch. Simulations assume a low level of muscle crossbridge cycling consistent with relaxed muscle. Length displacements were imposed on the muscle fiber. A) Predicted driving potentials (upper traces) during ramp stretches of varying velocity and acceleration (lower traces). B) Classical data showing Ia afferent firing modulation with different stretch velocity (Matthews 1963). C) Dynamic index emergent from crossbridge mechanisms. Dynamic index is defined classically as the ratio of firing rate at the end of the ramp phase and the firing rate 0.5 seconds into the hold phase (upper diagram). The muscle spindle model exhibits a sublinear relationship between dynamic index and stretch velocity (middle plot – colors correspond to A), similarly to classical findings (bottom plot). E) Linear acceleration scaling of initial burst emergent from crossbridge mechanisms. Initial burst amplitude is defined as the difference between peak firing rate during initial burst and baseline. Muscle spindle model exhibits linear scaling with stretch acceleration at stretch onset (top plot), which is consistent with classical findings (bottom plot – Schäfer 1969). Figures reproduced from Matthews (1963) and Schäfer et al. (1969).

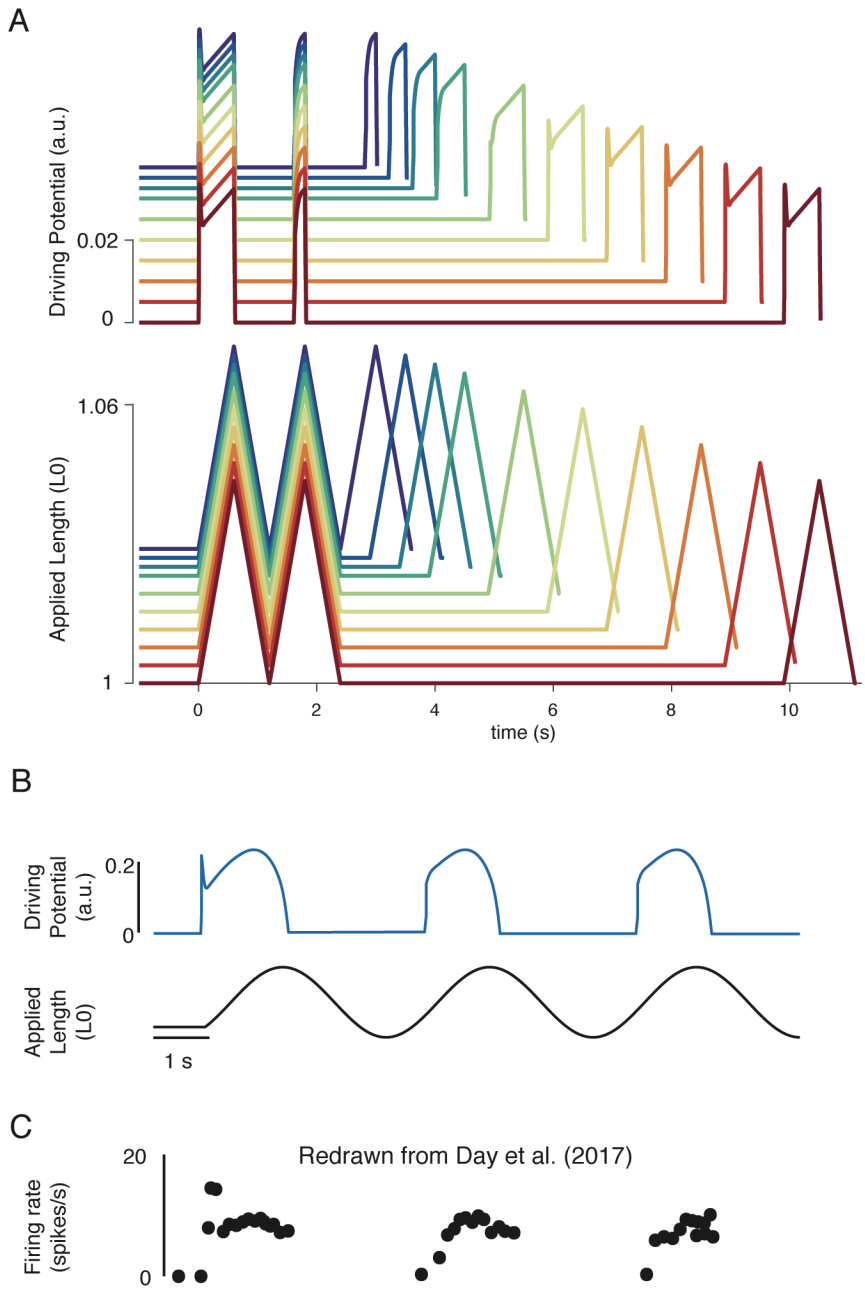

Figure 6 Emergent movement history-dependence of muscle spindle. A) When repeated stretch-shorten length cycles were applied, a larger response was predicted if the length was held constant prior to stretch (bottom plot – all traces). An abolished initial burst and reduced dynamic response were predicted in the second stretch, immediately applied after the length was returned to the initial value (top plot – all traces). In the third stretch, recovery of the initial burst was dependent on the time interval between the second and third stretch, with the effect saturating between 5-10 s (top plot, recovery from violet to red traces). This finding predicts the results found by Haftel et al. (2004) in rat muscle spindles. Similarly, dynamic response recovered gradually with time interval between second and third stretch (top plot, recovery from

violet to red traces). This finding predicts the results found by Proske and Stuart (1985) in toad muscle spindles. B) Sinusoidal displacement imposed from rest elicited a history-dependent initial burst in the predicted muscle spindle driving potential at the onset of stretch, resembling data from C) human muscle spindles recorded during the application of sinusoidal motion to the ankle in relaxed conditions (Day et al. 2017).

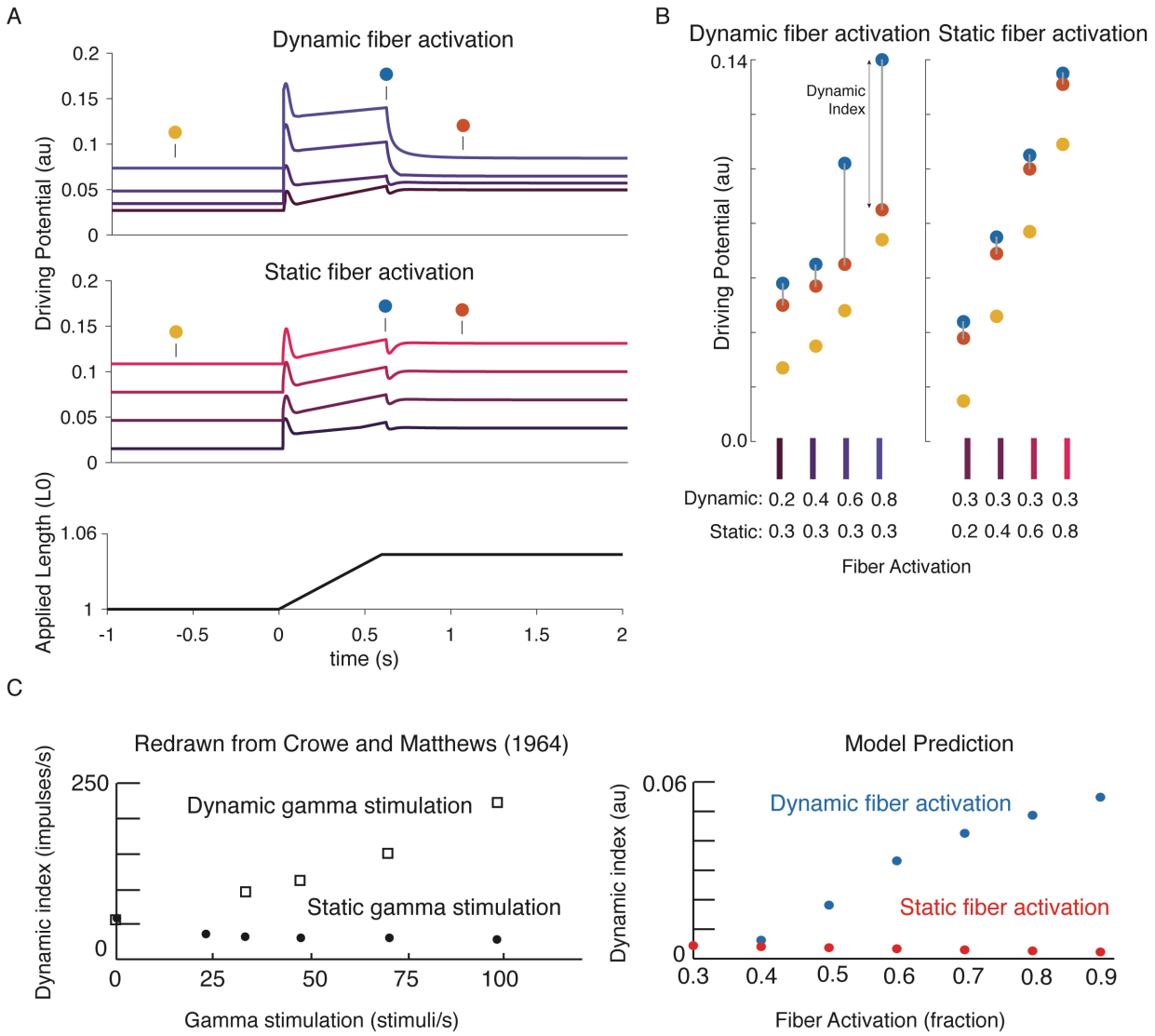

Figure 7 Changes in muscle spindle sensitivity caused by central drive emergent from interactions between dynamic and static fibers. Fusimotor activity was imposed on either the dynamic or the static fiber by increasing the number of active actin binding sites in the appropriate fiber. A) Simulated dynamic fiber activation increased the driving potential predominantly during the ramp, with smaller increases during the background and hold period (top traces). Simulated static fiber activation predominantly increases the driving potential rate during the background and hold period, with only modest increases in during the ramp. B) Emergent scaling of the dynamic index with dynamic (increase in dynamic index) and static fiber activation (decrease in dynamic index) resembled trends reported previously in the literature with C) dynamic index increasing with bag fiber activation, and dynamic index decreasing with chain fiber activation, respectively. Figures adapted and reproduced from Crowe and Matthews (1964) with permission.

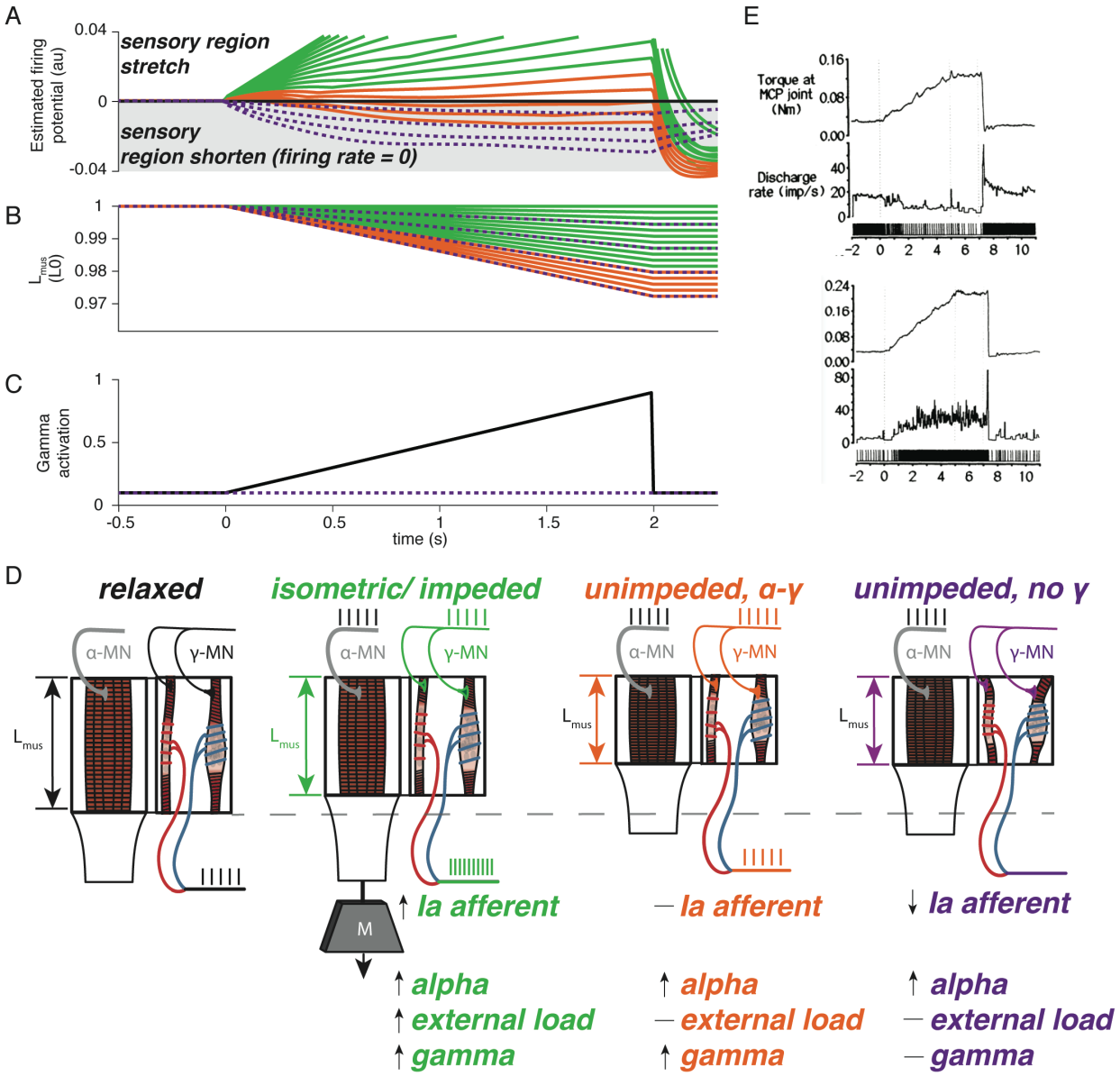

Figure 8 Paradoxical muscle spindle firing activity during isometric and shortening conditions emergent from intrafusal muscle mechanics. A-C) A spectrum of muscle spindle firing rates is predicted under different shortening and fusimotor conditions. When slow shortening is imposed on the spindle model under increasing fusimotor drive (black trace in C), muscle spindle firing increases (green traces in A-B). If spindle is shortened more rapidly, the firing rate may increase more slowly, not change, or even decrease (orange traces in A-B). If the spindle is shortened without fusimotor activation, the spindle firing rates will always decrease (dashed purple lines in A-C). D) Experimental conditions where these phenomena are expected. In a relaxed muscle spindle with no external loads, muscle spindle will exhibit a baseline firing rate (black). When central drive to the muscle and spindle are combined with an external load, the sensory region of the spindle is still stretched despite the overall shortening of the intrafusal fibers (green). If no external load is applied to the muscle with central drive, the sensory region of the spindle may increase slightly, decrease, or remain unchanged (orange). If central drive to the muscle is applied without fusimotor drive, the spindle will fall slack and decrease its firing rate. E)

Experimental examples of one muscle spindle decreasing its firing rate (top traces) and another increasing its firing rate (bottom traces) during an isometric task in human. Figure reproduced from Edin and Vallbo (1990) with permission.

REFERENCES CITED

1. Lin, D. C., McGowan, C. P., Blum, K. P. & Ting, L. H. Yank: the time derivative of force is an important biomechanical variable in sensorimotor systems. *Journal of Experimental Biology* **222,** jeb180414 (2019).

2. Blum, K. P., Lamotte D'Incamps, B., Zytnicki, D. & Ting, L. H. Force encoding in muscle spindles during stretch of passive muscle. *PLoS Comput Biol* **13,** e1005767–24 (2017).

3. Blum, K. P., Nardelli, P., Cope, T. C. & Ting, L. H. Elastic tissue forces mask muscle fiber forces underlying muscle spindle Ia afferent firing rates in stretch of relaxed rat muscle. *Journal of Experimental Biology* **222,** jeb196287–6 (2019).

4. Hunt, C. C. & Wilkinson, R. S. An analysis of receptor potential and tension of isolated cat muscle spindles in response to sinusoidal stretch. *The Journal of Physiology* **302,** 241–262 (1980).

5. Hunt, C. C. & Ottoson, D. Initial burst of primary endings of isolated mammalian muscle spindles. *J. Neurophysiol.* 1–7 (1976).

6. Haftel, V. K., Bichler, E. K., Nichols, T. R., Pinter, M. J. & Cope, T. C. Movement Reduces the Dynamic Response of Muscle Spindle Afferents and Motoneuron Synaptic Potentials in Rat. *J. Neurophysiol.* **91,** 2164–2171 (2004).

7. Getz, E. B., Cooke, R. & Lehman, S. L. Phase Transition in Force during Ramp Stretches of Skeletal Muscle. *Biophysical Journal* **75,** 2971–2983 (1998).

8. Hasan, Z. A model of spindle afferent response to muscle stretch. *J. Neurophysiol.* **49,** 989–1006 (1983).

9. Lin, C.-C. K. & Crago, P. E. Structural model of the muscle spindle. *Ann Biomed Eng* **30,** 68–83 (2002).

10. Schaafsma, A., Otten, E. & Van Willigen, J. D. A muscle spindle model for primary afferent firing based on a simulation of intrafusal mechanical events. *J Physiol* **65,** 1297–1312 (1991).

11. Mileusnic, M. P., Brown, I. E., Lan, N. & Loeb, G. E. Mathematical Models of Proprioceptors. I. Control and Transduction in the Muscle Spindle. *J. Neurophysiol.* **96,** 1772–1788 (2006).

12. Campbell, K. S. & Moss, R. L. A thixotropic effect in contracting rabbit psoas muscle: prior movement reduces the initial tension response to stretch. *J. Physiol. (Lond.)* (2000). doi:10.1111/j.1469-7793.2000.00531.x

13. Campbell, K. S. Dynamic coupling of regulated binding sites and cycling myosin heads in striated muscle. *J. Gen. Physiol.* **143,** 387–399 (2014).

14. Fukami, Y. Receptor potential and spike initiation in two varieties of snake muscle spindles. *J Physiol* (1978).

15. Hunt, C. C. & Ottoson, D. Impulse activity and receptor potential of primary and secondary endings of isolated mammalian muscle spindles. *J. Physiol.* (1975).

16. Matthews, P. Muscle spindles: their messages and their fusimotor supply. *European Journal of Neurology J2* - (1981).

17. Matthews, P. B. C. The Response of De-efferented Muscle Spindle Receptors to Stretching at Different Velocities. *J. Physiol. (Lond.)* **168,** 660–678 (1963).

18. Crowe, A. & Matthews, P. B. C. Further Studies of Static and Dynamic Fusimotor Fibres. *J Physiol* **174,** 132–151 (1964).

19. Boyd, I. A., Gladden, M. H., McWilliam, P. N. & Ward, J. Control of dynamic and static nuclear bag fibres and nuclearbag fibres and nuclear chain fibres by gamma and beta axons in isolated cat muscle spindles. *J. Physiol. (Lond.)* (1977).

20. Edin, B. B. & Vallbo, A. B. Muscle afferent responses to isometric contractions and relaxations in humans. *J. Neurophysiol.* **63,** 1307–1313 (1990).

21. Dimitriou, M. Human Muscle Spindle Sensitivity Reflects the Balance of Activity between Antagonistic Muscles. *Journal of Neuroscience* **34,** 13644–13655 (2014).

22. Gladden, M. H. & Boyd, I. A. *The Muscle Spindle*. (Stockton Press, 1985).

23. Meyer, G. A. & Lieber, R. L. Elucidation of extracellular matrix mechanics from muscle fibers and fiber bundles. *J Biomech* **44,** 771–773 (2011).

24. Bullinger, K. L., Nardelli, P., Wang, Q., Rich, M. M. & Cope, T. C. Oxaliplatin neurotoxicity of sensory transduction in rat proprioceptors. *J. Neurophysiol.* **106,** 704–709 (2011).

25. Emonet-Dénand, F., Laporte, Y., Matthews, P. B. C. & Petit, J. On the subdivision of static and dynamic fusimotor actions on the primary ending of the cat muscle spindle. *J. Physiol. (Lond.)* **268,** 827–861 (1977).

26. Jansen, J. K. S. & Matthews, P. B. C. The Effects of Fusimotor Activity on the Static Responsiveness of Primary and Secondary Endings of Muscle Spindles in the Decerebrate Cat. *Acta Physiologica Scandinavica* **55,** 376–386 (1962).

27. Song, Z., Banks, R. W. & Bewick, G. S. Modelling the mechanoreceptor's dynamic behaviour. *J. Anat.* **227,** 243–254 (2015).

28. Banks, R. W., Hulliger, M., Scheepstra, K. A. & Otten, E. Pacemaker activity in a sensory ending with multiple encoding sites: the cat muscle spindle primary ending. *J. Physiol. (Lond.)* **498 (Pt 1),** 177–199 (1997).

29. Poppele, R. E., Kennedy, W. R. & Quick, D. C. A determination of static mechanical properties of intrafusal muscle in isolated cat muscle spindles. *Neuroscience* (1979).

30. Gladden, M. H. in *Understanding the Stretch Reflex* **44,** 51–59 (Elsevier, 1976).

31. Houk, J. C., Rymer, W. Z. & Crago, P. E. Dependence of dynamic response of spindle receptors on muscle length and velocity. *J. Neurophysiol.* **46,** 143–166 (1981).

32. Schäfer, S. S. & Schäfer, S. Die Eigenschaften einer primären Muskelspindelafferenz bei rampenförmiger Dehnung und ihre mathematische BeschreibungThe characteristic of a primary …. *Pflügers Arch.* (1969).

33. Schäfer, S. S. & Kijewski, S. The dependency of the acceleration response of primary muscle spindle endings on the mechanical properties of the muscle. *Pflugers Arch - Eur J Physiol* **350,** 101–122 (1974).

34. Hasan, Z. & Houk, J. C. Transition in sensitivity of spindle receptors that occurs when muscle is stretched more than a fraction of a millimeter. *J. Neurophysiol.* **38,** 673–689 (1975).

35. Matthews, P. & Stein, R. B. The sensitivity of muscle spindle afferents to small sinusoidal changes of length. *The Journal of Physiology* **200,** 723 (1969).

36. Proske, U. & Stuart, G. J. The initial burst of impulses in responses of toad muscle spindles during stretch. *J. Physiol. (Lond.)* **368,** 1–17 (1985).

37. Hunt, C. C. & Wilkinson, R. S. An analysis of receptor potential and tension of isolated cat muscle spindles in response to sinusoidal stretch. *J Physiol* (1980).

38. Crowe, A. & Matthews, P. B. C. The effects of stimulation of static and dynamic fusimotor fibres on the response to stretching of the primary endings of muscle spindles. *The Journal of Physiology* **174,** 109–131 (1964).

39. Edin, B. B. & Vallbo, A. B. Dynamic response of human muscle spindle afferents to stretch. *J. Neurophysiol.* **63,** 1297–1306 (1990).

40. Lockhart, D. B. & Ting, L. H. Optimal sensorimotor transformations for balance. *Nat Neurosci* **10,** 1329–1336 (2007).

41. De Groote, F., Blum, K. P., Horslen, B. C. & Ting, L. H. Interaction between muscle tone, short-range stiffness and increased sensory feedback gains explains key kinematic features of the pendulum test in spastic cerebral palsy: A simulation study. *PLoS ONE* **13,** e0205763–21 (2018).

42. Maas, H., Gregor, R. J., Hodson-Tole, E. F., Farrell, B. J. & Prilutsky, B. I. Distinct muscle fascicle length changes in feline medial gastrocnemius and soleus muscles during slope walking. *J. Appl. Physiol.* **106,** 1169–1180 (2009).

43. Boyd, I. A. The response of fast and slow nuclear bag fibres and nuclear chain fibres in isolated cat muscle spindles to fusimotor stimulation, and the effect of intrafusal contraction on the sensory endings. *Q J Exp Physiol Cogn Med Sci* **61,** 203–254 (1976).

44. Husmark, I. & Ottoson, D. Ionic effects on spindle adaptation. *J. Physiol.* (1971).

45. Luu, B. L., Day, B. L., Cole, J. D. & Fitzpatrick, R. C. The fusimotor and reafferent origin of the sense of force and weight. *The Journal of Physiology* **589,** 3135–3147 (2011).

46. Jami, L. Golgi tendon organs in mammalian skeletal muscle: functional properties and central actions. *Physiological Reviews* **72,** 623–666 (1992).

47. Proske, U., Tsay, A. & Allen, T. Muscle thixotropy as a tool in the study of proprioception. *Exp Brain Res* **232,** 3397–3412 (2014).

48. Proske, U. & Gandevia, S. C. The Proprioceptive Senses: Their Roles in Signaling Body Shape, Body Position and Movement, and Muscle Force. *Physiological Reviews* **92,** 1651–1697 (2012).

49. Prochazka, A. & Gorassini, M. Ensemble firing of muscle afferents recorded during normal locomotion in cats. *The Journal of Physiology* **507,** 293–304 (1998).

50. Prochazka, A. & Gorassini, M. Models of ensemble firing of muscle spindle afferents recorded during normal locomotion in cats. *The Journal of Physiology* **507 (Pt 1),** 277–291 (1998).

327 **METHODS**

328 *Animal care*

329 All procedures and experiments were approved by the Georgia Institute of Technology's
330 Institutional Animal Care and Use Committee. Adult female Wistar rats (250–300 g) were studied in
331 terminal experiments only and were not subject to any other experimental procedures. All animals were
332 housed in clean cages and provided food and water ad libitum in a temperature- and light-controlled
333 environment in Georgia Institute of Technology's Animal facility.

334

335 *Terminal physiological experiments*

336 Experiments were designed to measure the firing of individual muscle afferents in response to
337 muscle stretch in vivo with electrophysiological techniques (e.g. Fig. 1). Rats were deeply anesthetized
338 (complete absence of withdrawal reflex) by inhalation of isoflurane, initially in an induction chamber (5%
339 in 100% O_2) and for the remainder of the experiment via a tracheal cannula (1.5–2.5% in 100% O_2). Surgical
340 and recording preparation followed by data collection lasted for up to 10 h. Subcutaneous injections of
341 lactated Ringer solution were given to support fluid levels and blood pressure. respiratory rate, Pco_2, and
342 core temperature were monitored via a rectal probe, and maintained between 36 and 38 °C with heated
343 water pads and a heat lamp. Pulse rate and Po_2 were monitored intermittently. At the conclusion of data
344 collection, rats were killed by exsanguination preceded either by overdose with isoflurane inhalation (5%).
345 Surgical preparation for data collection were described in earlier reports from this laboratory[51-53].

346 Briefly, the triceps-surae muscles nerves were dissected free of surrounding tissue in the left
347 hindlimb. All other nerves in the left hind limb were crushed to avoid (1) cross-talk with stimulation and
348 (2) to reduce total afferent feedback to the recorded dorsal root. The rats were fixed in a rigid frame at the
349 snout, vertebral bodies, distal tibia, and distal femur (knee angle 120°). The tendon of triceps-surae was
350 then cut at its insertion and attached to the lever arm of a force and length-sensing servomotor (Model
351 305C-LR, Aurora Scientific Inc.), which was used to control muscle length and measure force. Initial
352 muscle length was set at $L_{r(rest)}$. Dorsal roots exposed by laminectomy were placed on bipolar electrodes.

353 Triceps-surae nerves were loosely positioned in continuity on a unipolar silver stimulating electrode.
354 Exposed tissues were covered with warm mineral oil in pools formed by attaching the edges of severed skin
355 to the recording frame.

356 Either ramp-hold-release (e.g. Fig. 2B or repeated ramp release (e.g. Fig 2C) length changes were
357 applied to the muscle with the servomotor to evoke history-dependent stretch responses from the Ia
358 afferents. In the 11 afferents for which the initial pseudolinear model analyses were performed, a range of
359 6-99 stretch trials with varying maximum length and velocity were achieved depending on the recording
360 stability.

361 *Data inclusion and exclusion*

362 Analyses treated individual recorded afferents and individual recorded stretch trials as biological
363 replicates and as technical replicates, respectively. To ensure sufficient information for statistical measures,
364 we required that stretch trials have at least 50 recorded action potentials in order to be included in statistical
365 analyses. Stretch trials where spikes were not discriminable were excluded. These criteria yielded suitable
366 datasets for 11 individual afferents from 5 animals for pseudolinear model analyses and 6 individual
367 afferents from 5 animals for the axonal stimulation analyses. We also included 3 afferents from 3 animals
368 from a previous study in which the animal was treated with oxaliplatin[51].

369

370 *Muscle fiber force estimation*

371 To isolate the component of recorded musculotendon force arising from the muscle fibers (used as
372 a proxy for intrafusal muscle force), we assumed an idealized musculotendon mechanical arrangement (Fig.
373 1). In summary, we assumed there was noncontractile passive connective tissue arranged mechanically in
374 parallel with the muscle fibers and removed it analytically, as previously described[3].

375 Briefly, we assumed the noncontractile tissue acted as a nonlinear spring of the form:

376

377 $$F_{nc} = k_{lin}(L - L_0) + Ae^{k_{exp}(L-L_0)}$$

where k_{lin}, k_{exp}, and A are greater than or equal to zero. Once parameters were selected by the optimization procedure, the estimated noncontractile tissue forces were subtracted from the recorded force to estimate the muscle fiber force, which was fit to the IFRs.

Pseudolinear models for predicting firing responses

We predicted spiking responses using pseudolinear combinations of either recorded musculotendon length-related (length, velocity, and acceleration) or force-related (estimated muscle fiber force and yank) variables (Fig. S1). The relative weights and offsets for each variable in a model were optimized to minimize the squared error between the model prediction and Ia spike rates on a per-trial basis.

For both the force- and length-related models, we fit the estimated IFR for each model to the IFR of the afferent for each stretch trial included in our analyses (for all 20 afferents presented in this study). The model parameters, consisting of a weight (k_i) and offset (b_i) for each force- or length-related variable included in the sum, were found via least-squares regression using MATLAB's optimization toolbox (*fmincon.m*) and custom scripts.

We observed a peak to peak delay from the whole musculotendon yank and the initial burst, likely caused by delayed force transmission to the intrafusal fibers from the tendon[3]. A time delay (λ_j) was determined by shifting the timestamp of the variables forward relative to the IFR data to be fit (note: this time delay was 0 for all variables except yank, to account for the apparent delay between the onset of muscle force response and the onset of the spiking response). The general form of the models was:

$$IFR_{j,n}(t) = \left(\sum_{i=1}^{n} k_i \cdot \left(\lfloor x_i(t - \lambda_j) \rfloor + b_i \right) \right) \quad (1)$$

where the IFR estimate of the jth model for the nth perturbation was estimated by a sum of n force- or length-related variables, offset by a single value, b_i, and scaled by a gain, k_i. $\lfloor\ \rfloor$ denote positive values of the argument. Model estimates for IFR were related to the recorded IFR of the mth afferent by the equation:

$$IFR_{j,n}(t) + e(t) = IFR_{m,n}(t) \quad (2)$$

Error, $e(t)$, was minimized by finding the set of parameters for each model that minimizes a measure related to $e(t)^2$.

Axonal stimulation dataset

To test whether the force and yank components could arise from separate mechanosensitive mechanisms, another set of experiments was performed on 6 additional afferents in 4 animals. Each afferent dataset consisted of three trials in which the muscle was perturbed mechanically (3 mm, 20 mm/s). The first and third trials for each afferent served as bookend controls: alternating between control and intra-axonal current injection trials allowed assessment of the response through the course of extended single cell recordings. In the second of the three trials, we applied a depolarizing current (30nA for 500ms) which led to a train of antidromic action potentials traveling down the axon, which ceased immediately before applying a mechanical perturbation (3mm, 20mm/s), to which the firing response of the Ia afferents was dramatically reduced.

For each trial in these 6 afferents, we found the best-fit prediction for the force-related model using the parameter optimization described earlier. For the pre- and post-stimulation control trials, we first fit the model without a yank component, and then refit the model with a yank component. For the trials in which the electrical stimulus was applied, the yank component was set to be zero and the force and constant components were optimized as described before.

We performed one-way ANOVA on model performance (R^2), yank sensitivity (k_Y), force sensitivity (k_F), and the constant component (C) across 5 groups of model fits: pre-stimulus control trials without (1) and with (2) yank sensitivity, stimulus trials (3), and post-stimulus trials without (4) and with (5) yank sensitivity. We used the Tukey-Kramer method to examine all pairwise comparisons between groups.

Oxaliplatin dataset

We used data collected previously to test whether force and yank components were altered by oxaliplatin chemotherapy[51]. The effect of oxaliplatin on sensory coding of Ia afferents has been well-documented, so we analyzed three afferents from different animals. We fit the muscle fiber force-related model (described above) to three stretch trials for each afferent (3mm, 20 mm/s). We performed one-way ANOVA on model performance (R^2) between model fits with and without yank for each afferent to test the significance of the yank component on model performance.

Applying estimated fiber force-related driving potentials to model neuron

To test the feasibility of the force, yank, and constant components of the muscle fiber force-related model as mechanical signals encoded by the muscle spindle receptor, we applied a range of combinations of components to a conductance-based model neuron (based on the Connor-Stevens model; see next section) and examined the resulting firing rates. We first estimated the muscle fiber force and yank, as described previously, and varied the relative gains of these signals before adding them with a constant component. Once the components were added together, they were half-wave rectified, and applied to the model neuron as a stimulus current.

Model neuron sensitivities to these components were tuned until the model instantaneous firing rate was within 10 spikes/s for initial burst, dynamic response, and final plateau. We treated the parameter values which produced this response as the nominal values for the model. The relative sensitivities of the model neuron to force and yank component were then swept from 10-600% of their respective nominal values. We then compared the resulting changes in predicted firing rates with different phenotypical muscle spindle responses observed from these and other experiments.

Responses of muscle spindle Ia afferents to stretch

Consistent with prior studies, all Ia afferents exhibited initial bursts at onset of applied stretch, followed by a dynamic response during constant velocity stretch, and a period of rate adaptation during the

450 subsequent isometric hold period. When repeated ramp-release length-changes were applied to the muscle,
451 an initial burst and dynamic response was present during the first ramp, but the initial burst was absent and
452 dynamic response was reduced during subsequent stretches–a phenomenon in Ia afferents known as history-
453 dependence (cf.[54]).

454 The population of 11 Ia afferents considered for the first analysis varied in sensitivity to stretch
455 length, velocity, and acceleration. More dynamic afferents, as quantified by dynamic index (P. Matthews
456 1963) typically had relatively large spike responses during positive velocity stretch. More static afferents
457 exhibited more firing during the plateau phase of stretch, with relatively smaller dynamic indices. The
458 population of afferents also exhibited a range of initial burst amplitudes in response to stretch. There was
459 no clear relationship between the dynamic index and initial burst amplitudes for a given afferent. Despite
460 the differences in sensitivity amongst the afferent population, the waveforms of afferent responses to the
461 same stretch stimuli contained the same features (i.e. all afferents exhibited initial bursts, dynamic
462 responses, and rate adaptation to varying degrees).

463

464 *Conductance-based model neuron for reproducing spiking activity*

465 To demonstrate the plausibility of force- and yank-related ionic currents caused by stretch, we used
466 a modified Connor-Stevens conductance-based model neuron to model the transformation of graded
467 receptor potentials into action potentials by the afferent [55]. The model neuron contained a fast sodium,
468 delayed rectifier potassium, transient potassium, and leak conductances implemented in Simulink using
469 built-in differential equation solvers (ode23s.m).

470

471 *Intrafusal muscle model*

472 To simulate the hypothesized history-dependent mechanisms of intrafusal muscle fibers, we used
473 a computational model of crossbridge cycling. We implemented a model in MATLAB based on a simplified

474 structure of the model developed by Campbell[12,13,56,57], which incorporates the coupled dynamics between
475 myosin heads and actin binding sites (Supplemental Fig. 5).

476 *Intrafusal muscle model parameters*

477 Model parameters were either chosen to match the default parameters from Campbell[13] or chosen
478 so the model would exhibit history-dependence at the time-course measured in this work. All simulations
479 used the same set of model parameters (Supplemental Table S1).

480 Myosin attachment and detachment rates equations, $k_f(x)$ and $k_g(x)$, were selected such that the
481 force response of the model would exhibit history-dependent features consistent with observations in both
482 permeabilized muscle fibers and instantaneous firing rates of muscle spindle Ia afferents. Proske[58-60]
483 hypothesized that history-dependent muscle spindle IFRs (and corresponding perceptual errors) are caused
484 by a population of crossbridges within the intrafusal muscle that are unable to "keep up" with the rate of
485 shortening during an imposed movement, causing the intrafusal muscle fibers to fall slack. To model this
486 behavior, we selected rate equations that would produce relatively slow crossbridge reattachment during
487 shortening, but would retain other desired characteristics, such as short-range stiffness.

488

489 *Model of muscle spindle responses to stretch of intrafusal muscle*

490 To model the transformation of intrafusal muscle fiber stress into a firing waveform, we used a
491 pseudolinear combination of force and its first time-derivative, yank, based on previously published
492 observations [2]. Our model consists of two intrafusal muscle fiber models, a "static" fiber and a "dynamic"
493 fiber based on observations that muscle spindle primary afferent responses to stretch consist of two
494 components[2,19,28,43,61-65].. For these simulations, each muscle fiber model used identical parameters, but the
495 contribution of each fiber to the neural firing rate varied. The equation describing the contribution of each
496 fiber to the total firing rate is:

$$r(t) = r_{dynamic}(t) + r_{static}(t), \tag{15}$$

where the total firing rate of the afferent, $r(t)$, is a sum of the dynamic and static fiber components, or $r_{dynamic}(t)$ and $r_{static}(t)$, respectively. The static component was defined as:

$$r_{static}(t) = k_{Fs}\, F_s(t), \tag{16}$$

where k_{Fs} is a constant and $F_s(t)$ is the total force in the static fiber. The dynamic component was defined as:

$$r_{dynamic}(t) = \lfloor k_{Fd}\, F_d(t) + \, k_{\dot{F}d}\, \dot{F}_d(t) \rfloor, \tag{17}$$

where k_{Fd} and $k_{\dot{F}d}$ are constants, and $F_d(t)$ and $\dot{F}_d(t)$ are respectively the force and yank of the cycling crossbridges in the dynamic fiber. We used default k_{Fs}, k_{Fd}, and $k_{\dot{F}d}$ values of 1, 1, and 0.03, respectively, unless otherwise noted.

The static and dynamic fibers are arranged in perfect mechanical parallel and were allowed to be activated independently. Thus, the actions of the dynamic and static fibers could be simulated simultaneously or sequentially.

Occlusion between dynamic and static components

To account for the evidence of so-called "occlusive interaction" between dynamic and static branches of the muscle spindle Ia afferent ending, we used a nonlinear summation of the static and dynamic components. Previous models have used complete occlusion[9,66] but we used a partial occlusion based on more recent findings[28]. With occlusion, the total firing rate of the model Ia afferent becomes:

$$r(t) = \, f_{occ} r_{dynamic}(t) + r_{static}(t), \qquad r_{dynamic} \geq r_{static} \tag{18}$$

$$r(t) = \, r_{dynamic}(t) + f_{occ} r_{static}(t), \qquad r_{static} > r_{dynamic} \tag{19}$$

where f_{occ} is an occlusion factor limiting the contribution of either component to the overall firing rate. This parameter was set to 0.3 (unitless) for all simulations unless otherwise noted[28].

Dynamic response simulations

To demonstrate the ability of our model to produce the classical fractional power relationship between the dynamic response of muscle spindle Ia firing rates and ramp velocity[17,31,64], we applied a series

517 of ramp-hold stretches to the model with each fiber's proportion of available binding sites set to 0.3. The
518 ramp stretches consisted of a pre-stretch isometric hold period, followed by a constant velocity stretch that
519 varied linearly between trials from $0.079L_0$/s to $0.79L_0$/s, and another isometric hold period at its new length
520 ($1.059L_0$). The duration of stretch was shortened proportionally to the stretch velocity to ensure the same
521 total length was applied in each trial.

522 *Time-history dependence simulations*

523 To demonstrate the unique ability of our model to vary its own sensitivity to stretch based on the
524 history of movement applied to the muscle[54], we applied series of triangular ramp-release stretches with
525 each fiber's activation set to 0.3. Each series consisted of three stretch-shorten cycles, with a $1.047L_0$
526 amplitude and stretch and shorten velocities of $0.079L_0$/s. The first two cycles were applied sequentially
527 with no pause between them, whereas the third sequence was applied after a varied isometric hold period
528 at L_0 ranging from 0 – 10 s.

529 *Gamma activation simulations*

530 To demonstrate the effects of muscle activation on the firing response of our model, we applied a
531 range of activations to the static and dynamic fibers[25]. We varied the activation levels of the static and
532 dynamic fibers independently, between 0 – 1.0, before applying a $1.047L_0$ ramp-hold stretch at a constant
533 velocity of $0.079L_0$/s. We used k_{Fs}, k_{Fd}, and $k_{\dot{F}d}$ values of 1.5, 0.8, and 0.03, respectively, for these
534 simulations in order to better visualize the effects of gamma activation on the predicted driving potential.
535

536 *Human muscle spindle simulations*

537 To demonstrate the robustness of our mechanistic model to produce responses similar to those
538 observed in awake humans, we approximated stimuli from microneurography studies in humans from the
539 lower and upper limb. For the lower limb, we applied a $1.042\ L_0$ sinusoidal length change at 1.57 Hz to the
540 model at the baseline activation to mimic the passive manipulation of the ankle in the study[67]. To roughly

match the predicted driving potential to the firing rate of the spindle, we used k_{Fs}, k_{Fd}, and $k_{\dot{F}d}$ values of 1.8, 2, and 0.15, respectively.

For the upper limb, we applied ramp increases in gamma activation simultaneously with shortening ramps of the intrafusal muscle model in order to mimic the effects of putative alpha-gamma coactivation during an isometric task[68]. The linear increase in gamma activation approximated the linear increase in EMG recorded from the spindle-bearing muscle in human experiments. To mimic the shortening of the muscle due to tendon elasticity, we ran 8 separate simulations with different, but small, amounts of shortening of the model. Because of the unknown tendon elasticity in the finger muscles, we ranged the degree of shortening from 0 to 0.065 L_0/s during the activation stage of these trials.

Adaptation of previously published figures

Previously published results that were used for comparison with our model predictions were redrawn in Adobe Illustrator. Only single data points and lines were approximated by tracing over their apparent geometric centroids. These data were redrawn for aesthetic purposes only and were not used for any quantitative comparisons. Any comparison of data from these studies with the present study were performed using the original manuscripts.

ADDITIONAL REFERENCES

51. Bullinger, K. L., Nardelli, P., Wang, Q., Rich, M. M. & Cope, T. C. Oxaliplatin neurotoxicity of sensory transduction in rat proprioceptors. *J. Neurophysiol.* 106, 704–709 (2011).

52. Bullinger, K. L., Nardelli, P., Pinter, M. J., Alvarez, F. J. & Cope, T. C. Permanent central synaptic disconnection of proprioceptors after nerve injury and regeneration. II. Loss of functional connectivity with motoneurons. *J. Neurophysiol.* 106, 2471–2485 (2011).

53. Vincent, J. A. *et al.* Muscle proprioceptors in adult rat: mechanosensory signaling and synapse distribution in spinal cord. *J. Neurophysiol.* 118, 2687–2701 (2017).

54. Haftel, V. K., Bichler, E. K., Nichols, T. R., Pinter, M. J. & Cope, T. C. Movement Reduces the Dynamic Response of Muscle Spindle Afferents and Motoneuron Synaptic Potentials in Rat. *J. Neurophysiol.* 91, 2164–2171 (2004).

55. Connor, J. A. & Stevens, C. F. Prediction of repetitive firing behaviour from voltage clamp data on an isolated neurone soma. *The Journal of Physiology* 213, 31 (1971).

56. Campbell, K. S. & Lakie, M. A cross-bridge mechanism can explain the thixotropic short-range elastic component of relaxed frog skeletal muscle. *J. Physiol. (Lond.)* 510 (Pt 3), 941–962 (1998).

57. Campbell, K. S. & Moss, R. L. History-Dependent Mechanical Properties of Permeabilized Rat Soleus Muscle Fibers. *Biophysical Journal* 82, 929–943 (2002).

58. Proske, U., Morgan, D. L. & Gregory, J. E. Muscle history dependence of responses to stretch of primary and secondary endings of cat soleus muscle spindles. *J. Physiol. (Lond.)* 445, 81–95 (1992).

59. Proske, U., Tsay, A. & Allen, T. Muscle thixotropy as a tool in the study of proprioception. *Exp Brain Res* 232, 3397–3412 (2014).

60. Proske, U. & Gandevia, S. C. The proprioceptive senses: their roles in signaling body shape, body position and movement, and muscle force. *Physiological Reviews* 92, 1651–1697 (2012).

61. Jami, L. & Petit, J. Dynamic and static responses of primary and secondary spindle endings of the cat peroneus tertius muscle [proceedings]. *J. Physiol. (Lond.)* 296, 109P (1979).

62. Jami, L., Murthy, K. S. & Petit, J. A quantitative study of skeletofusimotor innervation in the cat peroneus tertius muscle. *The Journal of Physiology* 325, 125–144 (1982).

63. The structure and innervation of the nuclear bag muscle fibre system and the nuclear chain muscle fibre system in mammalian muscle spindles. *Phil. Trans. R. Soc. Lond. B* 245, 81–136 (1962).

64. Hasan, Z. A model of spindle afferent response to muscle stretch. *J. Neurophysiol.* 49, 989–1006 (1983).

65. Lewis, D. M. & Proske, U. The effect of muscle length and rate of fusimotor stimulation on the frequency of discharge in primary endings from muscle spindles in the cat. *J. Physiol. (Lond.)* 222, 511–535 (1972).

66. Hulliger, M., Matthews, P. & Noth, J. Static and dynamic fusimotor action on the response of Ia fibres to low frequency sinusoidal stretching of widely ranging amplitude. *The Journal of Physiology* 267, 811–838 (1977).

67. Day, J., Bent, L. R., Birznieks, I., Macefield, V. G. & Cresswell, A. G. Muscle spindles in human tibialis anterior encode muscle fascicle length changes. *J. Neurophysiol.* 117, 1489–1498 (2017).

68. Dimitriou, M. Human Muscle Spindle Sensitivity Reflects the Balance of Activity between Antagonistic Muscles. *Journal of Neuroscience* 34, 13644–13655 (2014).

SUPPLEMENTAL FIGURES AND LEGENDS

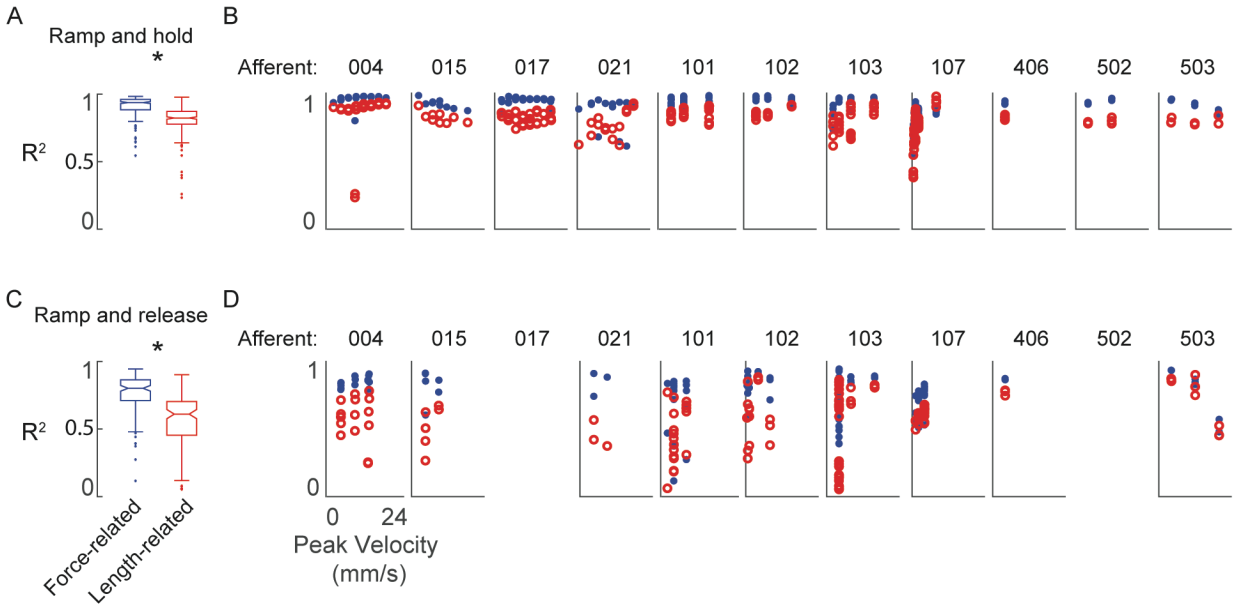

Figure S1 Goodness-of-fit to measured muscle spindle Ia afferent firing rates using estimated muscle fiber force and yank (blue) compared to kinematics model (red) as baseline comparison. A) Box and whisker plots of model goodness of fit (R^2) for all ramp-and-hold trials using estimated fiber force-based (blue) versus length-based (red) models. * denotes a significant difference between the model goodness of fit based on cumulative squared errors; $p<0.05$, one-way ANOVA. B) R^2 values for all individual trials of ramp-and-hold and within each afferent plotted versus stretch velocity for force-based (blue dots) versus length-based (red dots) models. C-D) Same as A-B, only for repeated ramp-release trials.

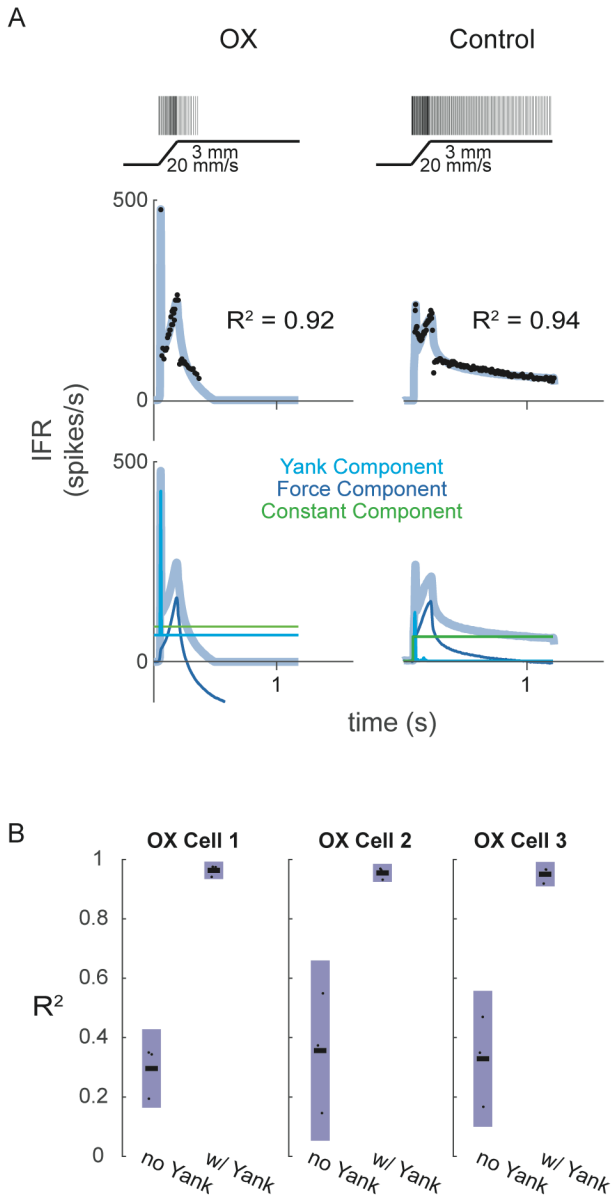

Figure S2
Fits of muscle spindle firing rates before and after oxaliplatin-induced neuropathy using estimated muscle fiber force and yank. (A) Example Ia afferent responses to stretch and force-based model fits. Left column shows a typical Ia afferent response to a ramp-hold stretch applied to the triceps surae of a rat treated with oxaliplatin chemotherapy (Bullinger et al. 2011). Right column shows typical response of Ia afferent in response to same ramp-hold stretch. Raster plots indicate times at which action potentials are recorded and are shown above imposed stretches. Below are the IFR and corresponding model fits shown above the same model fits with their respective components. (B) Variance of muscle spindle Ia afferent responses accounted for by force related model with (right bar in each plot) and without (left bar in each plot) yank for 3 Ia afferents from 3 oxaliplatin-treated rats. Black horizontal bars represent the means, blue bars represent the standard deviations, and black dots represent the data points from each trial (3 trials per afferent).

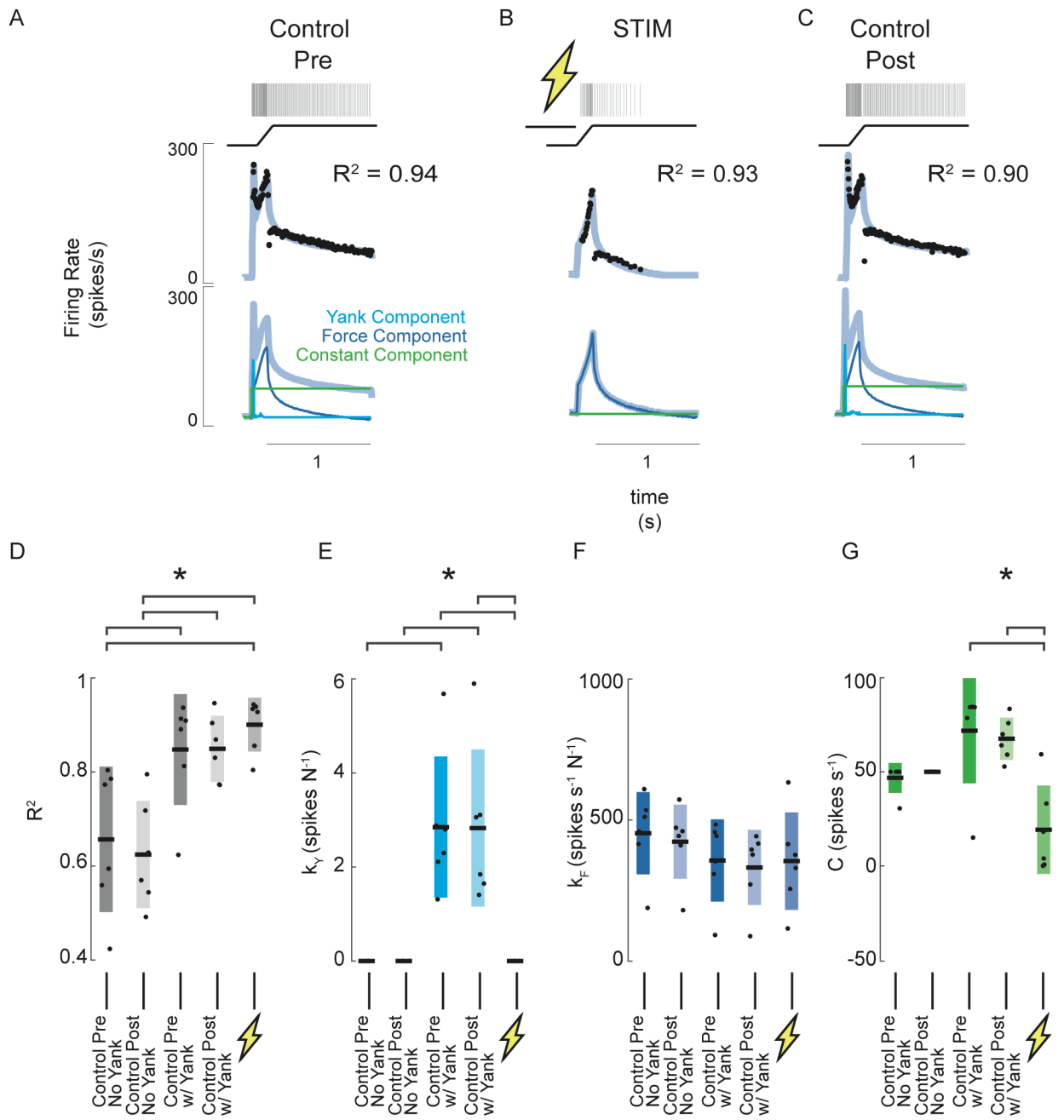

Figure S3

Estimated muscle fiber force-related model predicts changes in muscle spindle encoding caused by axonal stimulation. (A) Example of pre-stimulus control trial consisting of a 3 mm ramp-hold stretch at 20 mm/s. Raster represents the times of recorded action potentials in response to the ramp-hold stimulus shown directly below it. Black dots represent the afferent IFR corresponding to the raster. The gray-blue line represents the model prediction using force, yank, and constant components. Below this are the same model prediction as above (grey-blue) and model prediction components (blue – force component; cyan – yank component; green – constant component). (B) Example of stimulus trial consisting of the same stretch applied as A, with a depolarizing current applied to the axon directly prior to stretch. The model fit in this trial represents the best fit without the yank component. Notice the quality of fit does is roughly equal

in this trial with that of the pre-stimulus trial in A, but no yank component was necessary. (C) Example of post-stimulus control trial. Same stretch and model components were used as in A. (D) Goodness of fit (R^2) of force-related model for 6 afferents subjected to the same trials as shown in A-C. The first two columns show R^2 values of the model fits without yank components for the pre- and post-stimulus control trials, respectively, for all 6 afferents. The third and fourth columns from the left show R^2 values for the model fits with yank components for the pre- and post-stimulus control trials, respectively, for the same 6 afferents. The fifth column shows R^2 values for the model fits for the stimulus trials. This model did not use a yank component. (E) Model sensitivity to yank for the same model fits and afferents as D. (F) Model sensitivity to force for the same model fits and afferents as D and E. (G) Model constant component for the same model fits and afferents as D-F. Brackets above plots indicate significant differences between the means ($p < 0.05$).

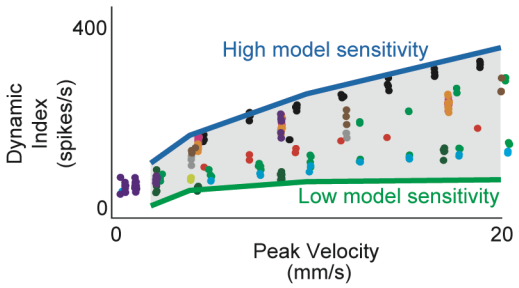

Figure S4
Estimated muscle fiber force model predicts inter-afferent variability of healthy afferent firing properties across perturbation velocity and acceleration. (A) Same dynamic index data shown in Figure 3-2 (colored dots) with predicted range of dynamic indices from model (gray shaded area). Nominal simulations were performed with the same force and yank model sensitivities for 4 stretch trials (2, 4, 10, 20 mm/s) from the same animal. Model parameter sweeps were performed for force and yank sensitivities for each of the 4 trials from 0.1 to 5 times the nominal value for each parameter. Green line represents the minimum dynamic indices from each of the 4 parameter sweeps from trials for which there was a spiking response (usually corresponding to low force and yank sensitivities). Blue line represents maximum dynamic indices from each of the 4 parameter sweeps (usually corresponding to high force and yank sensitivities). Gray shaded area represents plausible space of simulated dynamic index.

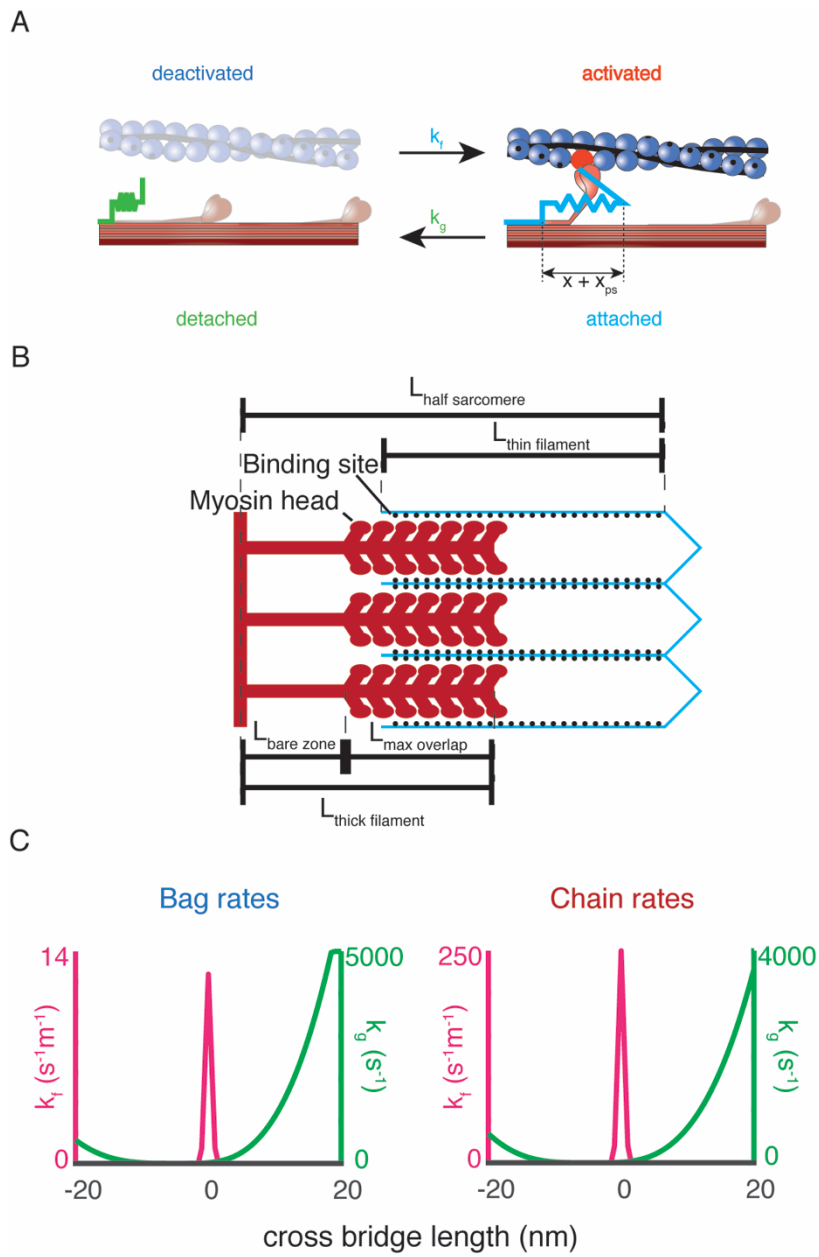

Figure S5
Biophysical intrafusal muscle models. A) Two-state dynamic system of cross bridge cycling. A population of detached cross bridges attaches at rate $k_f(x)$, and the population of attached cross bridges detaches at rate $k_g(x)$. When a cross bridge is formed at length x, an additional "powerstroke" length, x_{ps}, is applied to the cross bridge to generate a contractile force. B) Schematic of length variables accounted for in muscle model. The amount of overlap between the myosin heads of the thick filament (red) and actin binding sites of the thin filament (blue lines, black dots) is the relevant variable for the simulations. The fraction of overlap is simply the difference between the total length of the thick and thin filaments with the length of the half sarcomere, expressed as a fraction of the maximum potential overlap. C) Rate equations for myosin dynamics. The rate at which detached myosin

heads will attach as a function of the length, $k_f(x)$ of attachment is a Gaussian function, centered around 0 nm (shown in blue). The rate at which attached cross bridges will detach as a function of their length $k_g(x)$ is an offset polynomial function (shown in orange).

Parameter	Value (dynamic, static fiber)	Units	Description
k_{cb}	1	mN m^{-1}	Unit cross bridge stiffness
x_{ps}	2.5	nm	Unit power stroke distance
$L_{thick\ filament}$	815	nm	Length of thick filament
$L_{thin\ filament}$	1120	nm	Length of thin filament
$L_{bare\ zone}$	80	nm	Length of bare zone
$c_{filament}$	0.5	-	Filament compliance factor
ρ_{cb}	6.9×10^{16}	m^{-2}	Cross bridge number density
l_0	1050, 1200	nm	Passive force reference length
k_{pas}	100, 250	N m^{-2} nm^{-1}	Passive force linear stiffness

Table S1
Constant parameters used in both dynamic and static intrafusal muscle fiber models. These parameters did not change in any simulation presented in this study. When two values are presented, they represent the respective values for the dynamic and static fibers.